Universidade de Aveiro
2006

Department of Ceramics and Glass Engineering

Kingsley Odinaka Iwu

# Nanoencapsulation of Luminescent Lanthanide Complexes

Universidade de Aveiro
2006

Department of Ceramics and Glass Engineering
Joint European Masters in Materials(EMMS[1])

Kingsley Odinaka Iwu

# Nanoencapsulation of Luminescent Lanthanide Complexes

## Nanoencapsulamento de complexos lantanídeos luminescentes

A dissertation presented to the University of Aveiro in fulfilment of the requirement for the award of the European Masters degree in Materials Science under the supervision of Prof. Tito Trindade, of the Chemistry Department, University of Aveiro (with Prof. L.D. Carlos of the Physics Department acting as a co-supervisor), and Prof. Joachim Albrecht (Supervisor 2) of the Metallic Materials Department, Hamburg University of Technology

[1] EMMS is a joint exercise of the University of Aveiro (Portugal), Hamburg University of Technology (Germany) and Aalborg University (Denmark), run under the Erasmus Mundus scheme of the European Commission

**The Board of Examiners**

President

Dr. João Carlos Matias Celestino Gomes da Rocha
professor catedrático da Universidade de Aveiro

Dr. Luís Antonio Dias Carlos
professor catedrático da Universidade de Aveiro

Dr. Verónica Cortês de Zea Bermudez
professor associada da Universidade de Aveiro

Dr. Tito da Silva Trindade
professor associado da Universidade de Aveiro

**Acknowledgements**

My sincere gratitude goes to all those who contributed in one way or the other towards the completion of this thesis work. I will only attempt to say thanks to some of them here as much as time and memory permit me.

Firstly, I wish to thank the European Commission under whose sponsorship I am able to study in a truly European platform. I would also like to express my thanks to the entire coordination committee of EMMS across the 3 participating universities represented by Professor Ana Barros of the Department of Chemistry, University of Aveiro.

In the beginning, we bonded us together in order to sail through in an uncertain spin up and spin down weather; we deserves my deepest gratitude, especially those members of we who provided the critical ingredients that were definitely beyond my powers in those early days in Aveiro: many thanks to the first EMMS class at the University of Aveiro, and especially to the one Brazilian and Portuguese students. I will not fail to say thanks to the other students in the EMMS programme both in the first and second edition.

I would also like to thank some (senior) colleagues who shared time and space with me and had to put up with my many and seemingly never ending problems: Dr. Paula Soares Santos, Marcia Neves, Angela Pereira, Penka Girginova, Orley M. Ferri, and Jens Heidemann. The TEM people (if you know what I mean) at Hamburg University of Technology received the bulk of the external projection of my headache; I doff my cap to Ferhad Riazi, Jens Timmerman and Lida Wang.

Many thanks to my parents, Mr and Mrs S. C. Iwu, family members and to friends: Kingsley Nnaedozie, Kingsley Uzoma, Chinedu Nwakwue, Henry Mgbemere, Shylate Mahachi, and many others who time will fail me to mention.

Finally but not the least, I wish to thank my supervisors, Professors Tito Trindade, Luis Carlos and Joachim Albrecht.

**Palavras-chave** nanopartículas, luminescentes, complexos lantanídeos, óptica, micelas invertidas, sílica , titânia, bio-marcadores.

**Resumo**

Nanopartículas de sílica e titânia foram usadas para encapsulamento de complexos lantanídeos (Ln) de 3-hidroxipicolinato e picolinato, sintetizados por hidrólise de alcóxidos por meio de micelas invertidas – microemulsão de óleo em água, estabilizada com um agente surfactante, em que a fase aquosa existe na forma de domínios nanométricos. A alteração da dimensão destes domínios aquosos ou nano-reactores, conseguida variando a quantidade de água e mantendo constante a concentração de surfactante, determina aproximadamente o tamanho das partículas formadas no seu interior.

As características ópticas dos nano-compósitos tal como preparados, foi investigada e comparada com as de complexos lantanídeos puros, tendo em vista o seu potencial e futura aplicação como bio-marcadores. A microscopia electrónica de transmissão foi extensamente usada no estudo da morfologia dos nano-compósitos. Os resultados mostram que as propriedades luminescentes dos complexos de picolinato nos nano-compósitos foram severamente afectados pelo processo sintético, enquanto que os de complexos de 3-hidroxipicolinato nas matrizes, foram substancialmente distintos das suas propriedades originais. Estas propriedades ópticas foram correlacionadas com a estratégia sintética empregada e foram discutidas as suas implicações nas bio-aplicações em vista.

**Keywords** nanoparticles, luminescence, lanthanide complexes, optical, reverse micelle, silica, titania, bio-labels.

**Abstract**

Silica and titania nanoparticles encapsulating lanthanide (Ln) complexes of 3-hydroxypicolinate and picolinate were synthesized by the hydrolysis of alkoxides in a reverse micelle medium-water in oil microemulsion stabilized by a surface active agent (surfactant) in which the water phase exists as nanosized domains. The size of the water droplets or nano-reactors, which was varied by using distinct amount of water while maintaining constant the surfactant concentration, approximately determined the size of the nanoparticles formed therein.

The optical features of the as prepared nanocomposites were investigated and compared to those of the pure Ln complexes, having in mind their potential and future application as bio-labels. Transmission electron microscopy was chiefly employed to study the morphology of the nanocomposites. The results showed that the luminescence properties of the picolinate complexes in the nanocomposites were severely affected by the synthetic process while those of the 3-hydroxypicolinate complexes in the matrixes were markedly different from their original features. These optical properties were correlated to the synthetic strategy employed and the implication for the envisaged bioapplications discussed.

## Table of contents.

## Table of figures.

## Acronyms and definitions

| | |
|---|---|
| UV | ultraviolet |
| GS | ground state |
| ESS | excited singlet state |
| ETS | excited triplet state |
| NIR | near infra-red |
| UC | up conversion |
| PL | photoluminescent emission |
| PLE | photoluminescent excitation. |
| AOT | aerosol-OT (sodium bis (2-ethylhexyl) sulfosuccinate), $(C_9H_{17}O_2)_2CH_2CHSO_3Na$ |
| W/O | water-in-oil |
| Surfactant | surface active agent |
| TEOS | tetraethoxysilicate, tetraethoxysilane $Si(OC_2H_5)_4$ |
| QD | quantum dots, also called semiconductor nanocrystals |
| TRF | time resolved fluorescence |
| SBR | specific binding reagent |
| DLCLLA | direct lanthanide chelate label-based luminescence assay |
| DELFIA | dissociation enhanced lanthanide fluoroimmuno assay |
| EALL | enzyme amplified lanthanide luminescence |
| TP | titanium (IV) propoxide, $Ti(OC_3H_7)_4$ |
| DMSO | dimethyl sulfoxide, $(CH_3)_2SO$ |
| fwhm | full width at half maximum |
| APS | average particle size |
| PSR | particle size range |
| R | ratio of the concentration of water to that of surfactant |
| EuPic | 3-hydroxypicolinic acid complex of $Eu^{3+}$, $C_{18}H_{20}EuN_3O_{13}$ |
| TbPic | 3-hydroxypicolinic acid complex of $Tb^{3+}$, $C_{18}H_{20}EuN_3O_{13}$ |
| S/EuPic | composite material containing silica and EuPic. |
| S/EuPic-2 | S/EuPic nanocomposite prepared with an R = 2. The numbers after hyphen (-) in similar acronyms used in the text also stand for R |
| S/EuPic-2’ | S/EuPic-2 nanocomposite prepared by adding ammonia before TEOS, |

| | |
|---|---|
| | similar acronyms have similar meaning |
| S/Eu+Tb | nancomposite containing silica and a mixture of EuPic and TbPic |
| S/Eu0.5 +Tb0.5-4 | S/Eu+Tb in which the weight ratio of EuPic to TbPic is 0.5:0.5 and the R values is 4 |
| S/Eu0.3 +Tb0.7-6 | S/Eu+Tb in which the weight ratio of EuPic to TbPic is 0.3:0.7 and the R value is 6. Similar acronyms have similar meaning |
| 0.5Eu | 3-hydroxy picolinate heterocomplex in which the ratio of $Eu^{3+}$ to $Tb^{3+}$ is 0.5:0.5, $C_{18}H_{20}Eu_{0.5}Tb_{0.5}N_3O_{13}$ |
| 0.3Eu | 3-hydroxy picolinate heterocomplex in which the ratio of $Eu^{3+}$ to $Tb^{3+}$ is 0.3:0.7, $C_{18}H_{20}Eu_{0.3}Tb_{0.7}N_3O_{13}$ |
| 0.1Eu | 3-hydroxy picolinate heterocomplex in which the ratio of $Eu^{3+}$ to $Tb^{3+}$ is 0.1:0.9, $C_{18}H_{20}Eu_{0.1}Tb_{0.9}N_3O_{13}$ |
| S/0.5Eu | nanocomposite containing silica and 0.5Eu; similar acronyms have similar meaning |
| S/0.3Eu-8 | nanocomposite containing silica and 0.3Eu with R = 8. The same interpretation goes for similar acronyms |
| S/TbPic | nanocomposite containing silica and TbPic. |
| S/TbPic-10 | S/TbPic with R = 10, similar meaning goes for similar acronyms |
| T/EuPic | composite containing titania and EuPic |
| T/EuPic-2 | T/EuPic with R value of 2. Similar acronyms have similar meaning. |
| S-L | nanocomposite containing silica and lanthanide complex(es) |
| T-L | nanocomposite containing titania and lanthanide complex |

# Chapter 1. Introduction.

## *1.1. Luminescent lanthanides.*

### 1.1.1. Luminescence-an introduction.

Luminescence, in contrast to (infra) red emission which emanates from heating a solid to a temperature above 600 °C , is the emission of electromagnetic radiation (usually in the UV-visible and infra-red regions) by a material that has absorbed one form of energy or the other. The absorption of energy leads to the promotion of molecules to one or more excited states and a subsequent emission of radiation as the molecules return to the ground state (GS). The type of energy used in the excitation of a luminescent material can be broadly used to classify luminescent processes as photoluminescence, when the excitation is by electromagnetic radiation; cathodoluminescence, when a beam of energetic electrons is used; electroluminescence, when excitation is effected by an electric voltage; triboluminescence, when mechanical energy is the source of excitation; and chemiluminescence, when energy of a chemical reaction is employed [1].

The reason why all materials do not exhibit the phenomenon of luminescence, even though their molecules can be excited to a higher state, is that the return to the ground state radiation process has a competitor in non-radiation return to the ground state. This is the typically the case when the vibration energy level of the excited state is close to a ground state (GS) vibration energy level, thus providing the excited molecules with an alternative and otherwise convenient pathway to return to a stable energy level. This transition from the vibration energy level of an excited state to the vibration energy level of a GS is called internal conversion; the absorbed energy, rather than being emitted, is used to excite the vibrations of the molecules or host lattice.

Light emission can be classified as fluorescence, which is usually short lived ($10^{-7}$-$10^{-9}$ s) and does not involve a change of electron spin in the transition (ESS to GS), or phosphorescence, when the emission is much longer (10-$10^{-3}$ s) and involves a change of spin

during the transition from an excited triplet state (ETS) to the ground state. The ratio of radiation to non radiation return to the ground state indicates the efficiency of the luminescent material [2]. Hence population of an excited state and the energy difference between the GS and excited states are among the important factors that affect the luminescence of a material. Figure 1 gives an illustration of some of the typical processes involved in luminescence. In the course of this thesis report, fluorescence will be loosely used to refer to both type of luminescent emission at times.

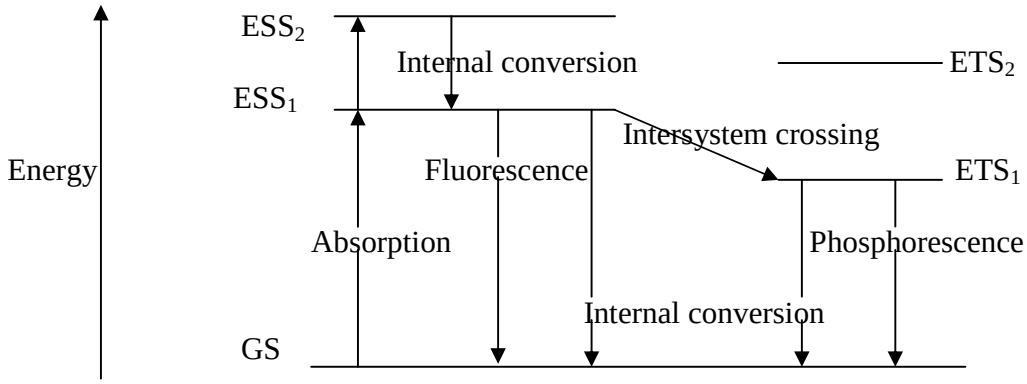


*Fig. 1.1: Energy absorption by a material and subsequent ways in which the absorbed energy can be released. Note that internal conversion can also occur between the energy levels of two ESS levels and between an ETS and the GS. Intersystem crossing is a process by which a molecule in an ESS transits to an ETS. Absorption from a GS directly to an ETS is forbidden.*

### 1.1.2. The Lanthanides and their optical properties.

The elements from cerium (Ce, z = 58) to lutetium (Lu, z = 71) make up what is known as the lanthanide series of the periodic table (lanthanum, La, is considered in some quarters to be the beginning of the lanthanide series). They, together with scandium (Sc), yttrium (Y) and at times the actinides, are often referred to as rare earth elements, which is somewhat erroneous considering that even the most scarce rare earths (e.g., europium, lutetium) are more common than the platinum-group metals. The lanthanides have a strong resemblance among

themselves in their chemical properties, with the $Ln^{3+}$ as their predominant oxidation state [3-4]. Optical based applications for lanthanides are based on their unique optical properties and are in such areas as the fields of lightning, cathode ray tubes, lasers and light emitting diodes, optical amplifiers in telecommunication, and biological sensors for medical diagnosis [1, 5-9].

The unique optical properties in question include their sharp (high purity) and intense intra 4f emissions, large Stokes shifts, long luminescence life time and resistance to photo-bleaching [7, 10-11]. Induced electric dipole transition between energy levels with the same parity such as electronic transitions within the d-shell, within the f –shell and between the d and s shells are forbidden by the parity selection rule. However, since the 4f shells of a lanthanide ions lie within and are shielded from the surrounding of the lanthanide ion by the completely filled $5S^2$ and $5P^6$ shells, the selection rule appears relaxed and so intra 4f transitions are witnessed in $Ln^{3+}$, resulting in sharp spectral emission and longer lifetime. However, some level of interaction exists between a lanthanide ion and its crystal field which makes it possible for the spin selection rule which forbids electronic transition between levels with different spin to be negated: the intra 4f electronic transitions in lanthanides involve levels with opposite spin, example the $^5D_0$- $^7F_J$ transitions in europium (where J is the total angular momentum and its value is given by the addition of the spin (S) and orbital (L) angular momenta if the 4f orbital is more than half filled or L minus S when the orbital is less than half field). The spin selection rule becomes broken when opposite-parity wave function of higher energy electronic states are mixed into the 4f wave functions, a mixing that allows the 4f-4f transitions to enhance their probability by drawing from the intensity of the higher electronic states [1-2, 12]. In addition to the splitting of the energy of the 4f orbital by spin-orbit coupling, individual J levels of a lanthanide ion are split further by the crystal field into 2J+1, making the emission of lanthanides extremely sensitive to their environments.

Even with the selection rules relaxed, lanthanide ions are still poor absorbers of energy and so cannot be excited directly in an efficient manner [8, 10, 13]. To overcome this problem, the lanthanides must be sensitized via their surrounding and it is the sensitization attempt that defines the preparation of the molecular structures in which the lanthanides are housed.

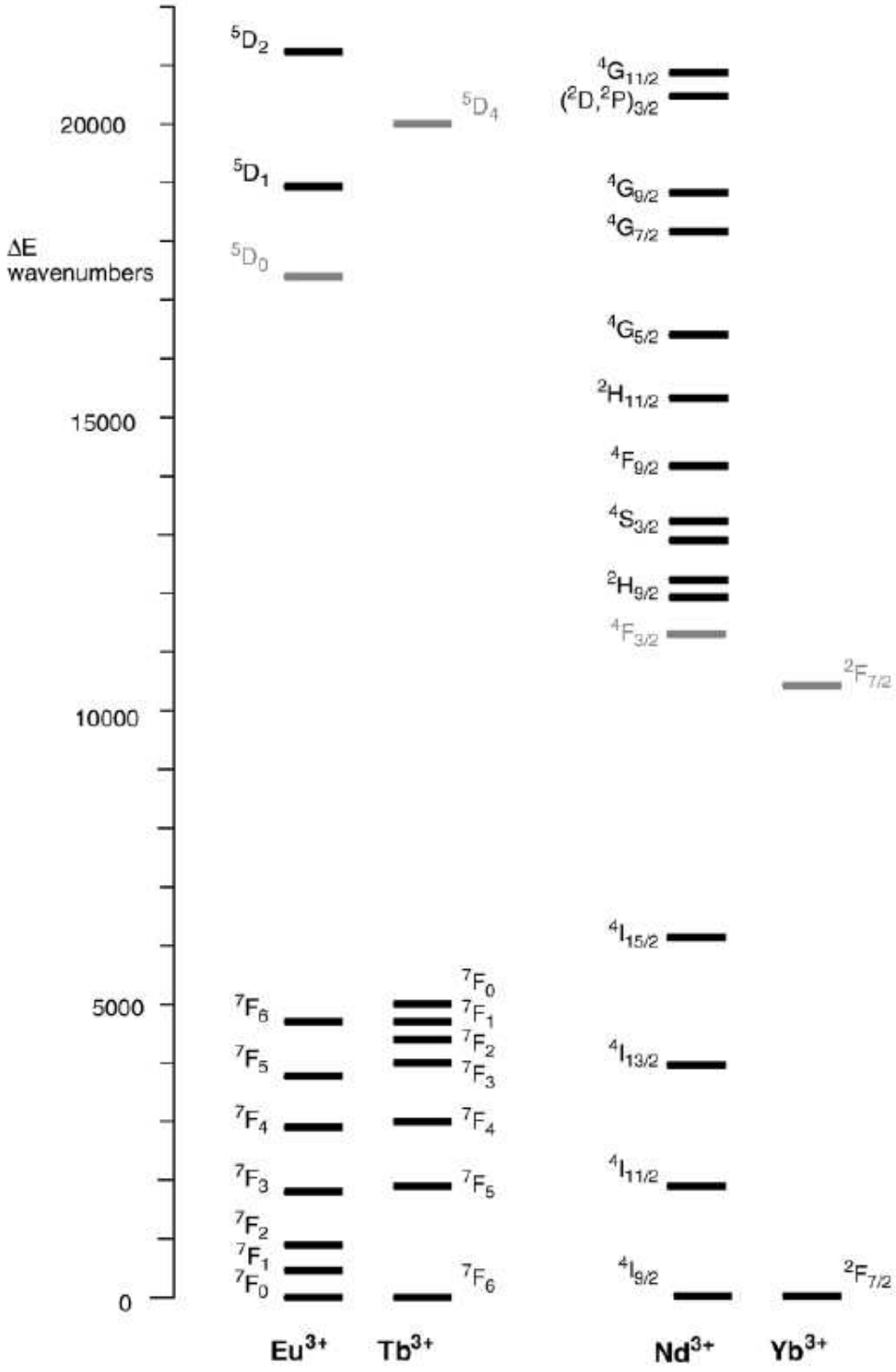


*Fig. 1.2: Energy level diagram for some lanthanides*

The overall quantum yield of a lanthanide containing molecule can then be summarized thus:

$$Q^{L}_{Ln} = \eta_{sens} Q^{Ln}_{Ln} \qquad 1.1$$

Where $Q^{L}_{Ln}$ and $Q^{Ln}$ Ln are the quantum yields of indirect and direct excitation respectively and $\eta_{sens}$ represents the efficiency of the transfer of energy from the sensitizer or antenna to the lanthanide ion [2]. The molecular structures that incorporate lanthanide ions towards realizing efficient sensitization can be generally identified as:

### 1.1.2.1. Inorganic phosphors.

The first and most prominent group of lanthanide based inorganic phosphors are oxides of lanthanides, [12,14] or (mixed) oxides of other rare earth elements with the emitting lanthanide as a dopant. [5, 7, 11, 15-17]. Rare earth oxysulfides [18] and rare earth fluorides such as $LaF_3$ [19] $YF_3$ [20], and $NaYF_4$ [21-23] are also reported as good hosts for lanthanides. Here the emitting lanthanide is called an activator while the sensitizer can be another dopant (usually a lanthanide), the host lattice or even the activator itself (in the case of a pure compound of the lanthanide). If we consider the sensitizer in a lattice to be a certain ion $A^{3+}$, and the emitting lanthanide ion as $B^{3+}$, the energy absorption, transfer and emission processes can be depicted by the following equations:

$$A^{3+} + h\nu = (A^{3+})^* \qquad 1.2 \text{ - absorption}$$

$$(A^{3+})^* + B^{3+} = A^{3+} + (B^{3+})^* \qquad 1.3 \text{ - energy transfer}$$

$$(B^{3+})^* = B^{3+} + h\nu \qquad 1.4 \text{ - lanthanide emission}$$

* represents an excited state and hν stands for photon energy.

$YF_3$, $NaYF_4$ and a variety of rare earth oxysulfides and oxides can exhibit an anti-Stokes phenomenon called *up conversion* (UC) when doped with $Er^{3+}$ and/or $Yb^{3+}$ [3+, 21-22, 24]. UC is the generation of one higher energy visible photon from at least two lower energy near infra-red (NIR) photons and its initiated when an excited ion transfers its energy to a neighbouring ion

which is also in an excited state; the transfer step can be in one or more steps, that is, the emitting lanthanide ion (usually $Er^{3+}$) can receive more than one photons. Yet another interesting optical phenomenon which is the exact opposite of UC is exhibited by quantum cutting phosphors. Here a photon absorbed by one lanthanide is transferred to two other different lanthanides and thus lead to an emission of two photons. Examples of such an occurrence is seen in one photon vacuum ultraviolet absorption by $Gd^{3+}$, transfer of the energy to two different $Eu^{3+}$ centres which then emit in the red region of the visible, and one visible photon absorption by $Tb^{3+}$, followed by transfer of the energy to two $Yb^{3+}$ ions and subsequent two NIR emission. Quantum cutting phosphors are said to be promising for high energy efficiency because they can lead to a red shift in emission of the absorbed energy with no energy dissipated, in contrast to the current phosphors in lightning and display applications which dissipate as much as 50% of absorbed energy in the form of heat [17].

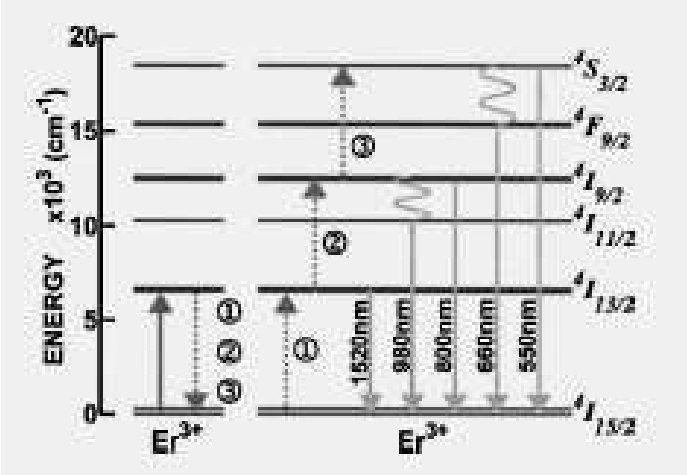


*Fig. 1.3: UC process between two erbium $Er^{3+}$ ions. Energy relaxation from one $Er^{3+}$ ion (the sensitizer) can result in energy transfer to a neighbouring $Er^{3+}$ ion (activator) giving rise to higher energy photons, and the energy transfer can be in one or multiple steps. Solid lines represent photon absorption (up) and emission (down), dotted lines represent energy transfer, wavy lines represent phonon emission* [21]

### 1.1.2.2. Lanthanide complexes.

These are compounds in which Ianthanide ions are dative-coordinated to other molecules, usually called ligands. The ligands, which are mostly organic molecules, are responsible for absorbing energy and transferring them to the lanthanides ions. It is a common thing to design a lanthanide complex or chelate to have a coordination number greater than six, with all coordination to the organic ligands, excluding water molecules from the primary coordination sphere. The reason for the attempt to exclude water from the coordination sphere of the lanthanide is said to be that water is highly detrimental to the luminescence of the excited lanthanide state by way of vibration energy transfer from the lanthanide's ETS to O-H [2, 25-26]. However, Bunzli et al [27], and Trindade et al [3-4, 13] have reported luminescent lanthanide chelates with water molecules in the primary coordination sphere of the lanthanides. Other oscillators that are reported to be potential quenchers of the luminescence of lanthanide ions include N-H and C-H stretching vibrations [26].

Some of the ligands that have been reported in literatures as capable of absorbing photons and transferring to $Ln^{3+}$ ETS include (substituted) molecules like nicotinate, with Eu, Gd, Tb, Er, and Tm [13]; picolinates, with Eu, Tb and Er [4, 9] ; benzoates, with Sm and Tb [3]; nicotinate-phenanthroline, with Tb [28]; trifluoroacetylacetone-triphenylphophine, with Gd [29]; 1-Dodecyl-3-methylimidazolium chloride, with Eu [30] (a room temperature ionic liquid with potential application as a liquid crystal display, LCD); poly(pyrazolyl)borates, with Pr, Nd, Er, and Yb, [31-32]; tropolonate, with Nd, Er, Ho, Tm and Yb [33]; terpyridines, with Eu and Tb [27, 34-35]; 7-aceyoxy coumarin 3-carboxylic acid and 1-(4-methoxyphenyl) 3-(4-t-butyl phenyl) 1,3-propandione, with Sm [25]. On the other hand, more complex molecules have been used as ligands, namely: dendrites such as dendritic β-diketone (benzoyltrifluoroacetone units with poly aryl ether dendrons), with Eu [8]; polymers such as poly (2-(6'cyano-6'methyl-heptyloxy)-1, 4- phenylene) with Eu [36]; macrocycles with Eu [37-38]; an inorganic metal-oxide clusters (polyoxometalates), with Eu, Tb, Sm and Dy [39]; and a complex polymer-dendrite comprising aromatic carbonyl amide and nitrate ion repeating units, with Tb; the latter exhibiting a NIR excitation-green emission UC [40]. The complexes used in this work were 3-hydroxypicolinates and picolinates of $Tb^{3+}$ and $Eu^{3+}$.

The use of lanthanides complexes may as well be desirable for keeping the lanthanide ions well separated from each other in order to avoid concentration self-quenching of luminescence; this is also another advantage of using doped inorganic phosphors in which the activator is the dopant [7]. Just like in inorganic phosphors, an interesting phenomenon of energy transfer between two different lanthanide ions in the same molecular complex which enhances the luminescence of the emitting ion has been reported.[20, 29].

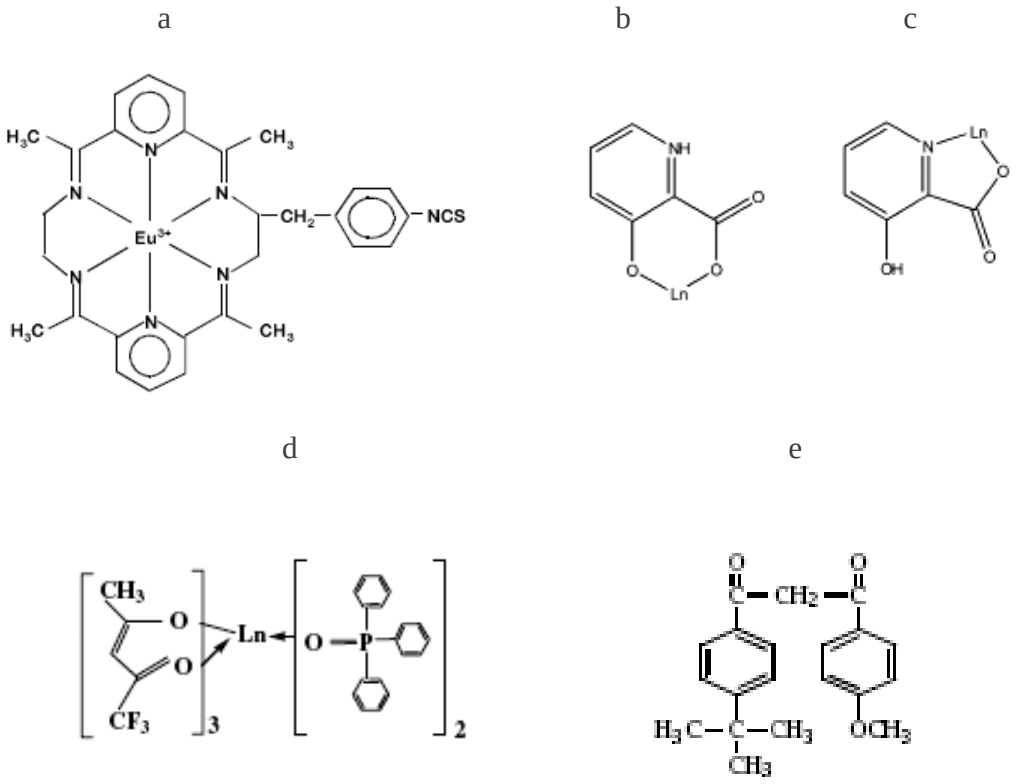


*Figs. 1.4: a. A macrocyclic- Ln complex [19]; b. 3-hydroxypicolinic acid-Ln complex with N, O-chelation to give a six-membered chelate ring, and c: analogous 3-hydroxypicolinate-Ln complex with a O, O chelation giving a five-membered ring [4]; d. trifluoroacetylacetone/triphenylphophine oxide- Ln chelate [16]; e. 1-(4-methoxyphenyl) 3-(4-t-butylphenyl) 1,3-propandione ligand for $Sm^{3+}$ [25]*

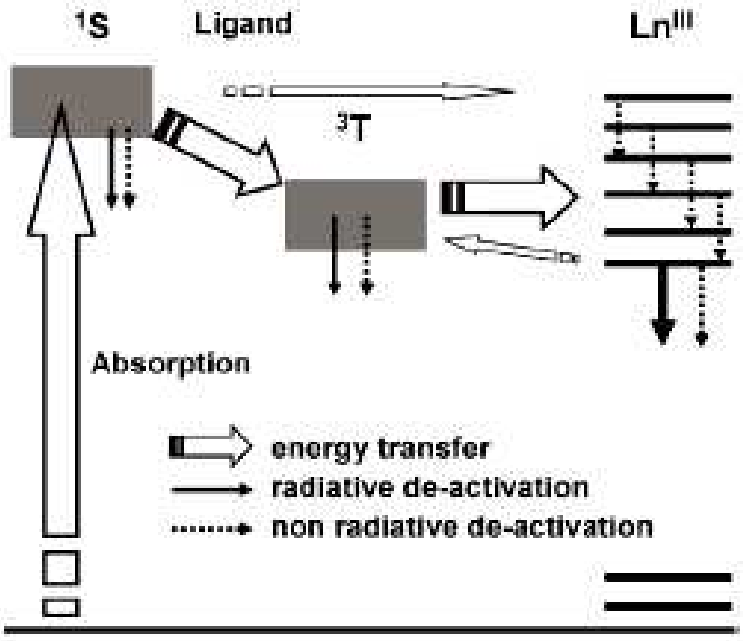


*Fig.1. 5: The antenna effect, the ligand absorbs energy to get to the ESS (1S), undergoes intersystem crossing to its ETS (3T), and transfers its energy to the ETS of the $Ln^{3+}$ which then relaxes into is GS state with an emission.*

## *1.2. Silica ($SiO_2$) and titania ($TiO_2$) nanoparticles*

Silica and titania prepared as either nanosized or bulk materials and with varying degrees of porosity are widely applied in several areas. Silica is used in such areas as glass preparation, catalysis, chromatography, automotive, electronics, sensors, rubber products and plastic binders [41-42]. Titania has found wide application in photocatalysis [43-45] and photoelectrical energy conversion [45]. In addition, it has strong potential for gas sensing [46], optics [47] (due to its high refractive index) and as an adsorbent for the removal of heavy metals from aqueous solution [48]. Due to their biocompatibility, they both have good potentials for bio-applications [49-50]. In recent times, there has been an explosive interest in nanostructured materials, and those of silica and titania are no exceptions. Silica and titania nanosized particles will henceforth be of primary concern in the rest of this thesis.

Both bulk and nanosized particles of silica and titania have been made by the hydrolysis and subsequent polycondensation of their respective metal alkoxides (including their organic-modified counterparts) [4, 48, 51]. This process is also applied in producing other technologically important metal oxides [48] and also forms the backbone of the all important sol-gel synthetic method [48, 52-56]. For silica, the use of aqueous ammonia solution as a catalyst yields spherical nanoparticles while bulk materials have been obtained with only water [4, 57-58]. Careful control of the fast paced titania alkoxide hydrolysis by the use of a polymeric stabilizer or ionic agent (e.g. NaCl) can lead to titania nanoparticles [47-48]. In addition, titania nanoparticles have also been prepared by controlled hydrolysis of titanium tetrachloride [45] and oxidation of a titanium ion containing surface active agent (surfactant) in a water-in-oil microemulsion [59].

The preparation of silica and titania, and indeed other metal oxides, from metal alkoxides or their derivatives takes place in 2 stages. First the precursor is hydrolysed to form the hydroxide which subsequently undergoes a polycondensation reaction to give the oxide [42, 57]

$$M\text{-}(OR)_n + nH_2O = M(OH)_n + nROH \qquad \text{1.5-hydrolysis}$$

$$M(OH)_n = MO_{n/2} + n/2H_2O \qquad \text{1.6-polycondensation}$$

## *1.3. Water-in-oil microemulsions (reverse microemulsions) and nanoparticles*

A microemulsion is an isotropic and thermodynamically stable solution of two immiscible liquids that are brought into a single phase by a surfactant. They are macroscopically homogenous but microscopically heterogeneous because two domains-oil and water rich- are separated by a surfactant.[51, 59]. The minor phase usually exists as spherical, cylindrical or sponge-like nanosized domains [60], sometimes referred to as nanoreactors because nanosized colloidal organic (including pharmaceuticals and polymers) and inorganic particles can be produced in their interior [60-61]. Those nanosized domains are called micelles (reverse micelle

for water-in-oil) because they consist of an aggregation of surfactant molecules surrounding and stabilizing the minor phase droplets.

In recent times, water-in-oil microemulsions, W/O, or reverse micelles have become very important and widely used in the preparation of nanoparticles, owing mainly to their ability to yield monodispersed particles.[20, 59, 62-65]. They also offer the possibility of tuning the sizes of nanoparticles by varying the ratio of the concentration of water to that of the surfactant according to: [62, 66]

$$R = [H_2O]/[SURFACTANT], \qquad 1.7$$

where R is the particle size and the terms in parenthesis are concentrations.

Thus keeping other parameters constant and using different amounts of water for a fixed concentration of the surfactant, different sizes of nanoreactors/nanoparticles can be generated.

The water/Aerosol-OT, AOT (sodium bis(2-ethylhexyl)sulfosuccinate)/Alkane system is the most widely studied reverse microemulsion [66-68], and is generally believed to yield spherical nanopools of water even when the sodium ion is replaced by divalent cations [69 a]. AOT comprises two alkyl tails, which extend to the organic phase in a W/O microemulsion and a negatively charged head group (with the $Na^+$ as a counter ion). The head group ions bond to and stabilize the water pool. It has been reported that the number of water molecules per AOT molecule reaches a maximum value of about 12, for R = 18, and that beyond this R value, the number of free water molecules increases sharply [67].

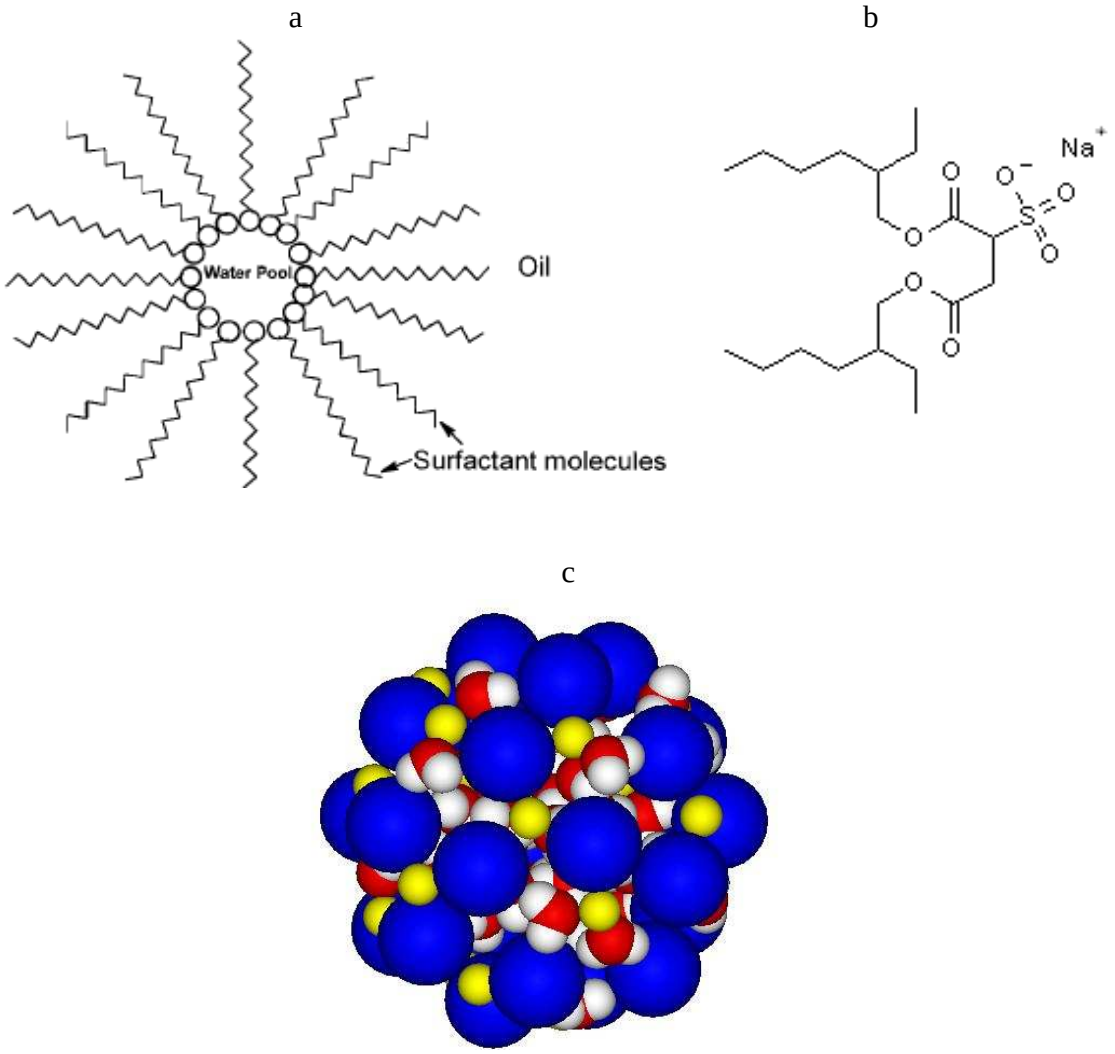


*Figs.1. 6: (a) Scheme of a reverse micelle in an oil phase formed by the aggregation of surfactant molecules around a water droplet. The water droplet (water pool) is nanosized and hence acts as a nanoreactor for material synthesis [62]. (b) AOT molecule showing the two branched alkyl groups and the anion head ($SO^{3-}$) with the sodium counter ion. In a typical W/O microemulsion, the head group attaches to water molecules while the alkyl groups extend to the oil phase. (c) A model of a reverse micelle for AOT [69 b]. Blue—head group anions ($SO^{3-}$), red—water oxygen, white—water hydrogen, yellow—$Na^{+}$.*

### 1.3.1. Nanoparticles and nanoreactors.

Since the classical sol-gel preparation of silica and (mixed) metal oxides involves hydrolysis of alkoxides or their derivatives, the water pool in a W/O system offers a good base for the preparation of oxide nanoparticles capped. The range of oxides and other inorganic nanoparticles prepared in reverse micelles are varied and include silica [51, 62], titania [59], perovskite oxides such as $BaPbO_3$, $BaTiO_3$, $SrZrO_3$, $LaNiO_3$, $La_2CuO_4$ and $Pb(Mg_{1/3}Nb_{2/3})O_3$ [70]; semiconductor nanocrystals such as PbS [71], $Cd_{1-x}Mn_xS$, $Cd_xZn_{1-x}S$ [60] and ZnO [63]; metal nanoparticles such as gold [68] and silver [72]. The list is not limited to inorganic materials as organic nanoparticles such as cholesterol, rhodiarome, rhovanil and nimesulide have been prepared in reverse micelles [61]. The robustness of reverse micelle can be further seen in the various synthetic methods employed therein to make the nanoparticles: from hydrolysis of alkoxides to give silica and titania and hydrolysis of $TiCl_4$ to give titania [51], to reduction of salts to give Au [68] and Ag [72], double displacement reactions to give PbS [7I] and $BaSO_4$ [64], hydrolysis of nitrates of $Pb^{2+}$, $Mg^{2+}$ and $Nb^{5+}$ to yield their hydroxides which were later heat-treated to get perovskite $Pb(Mg_{1/3}Nb_{2/3})O_3$ [70], and to replacement of the $Na^+$ counter ion of AOT by $Ti^{4+}$ followed by hydrolysis in a reverse microemulsion to yield titania [59].

Another fine feature of reverse micelles is their handiness in developing encapsulating nanomaterial, a sort of nanoparticle in a nanoreactor. Due to some limitations associated with nanoparticles such as dangling bonds, toxicity, hydrophobicity, rough surfaces, and generally, the need to provide housing for them and thus make them pliable in usage [20, 57], encapsulation in another (nano)structure is desirable. Reverse micelles have been effectively employed to encapsulate semiconductor nanocrystals [57, 73, ]. $YF_3$ nanoparticles [20], and luminescent organic dyes [62] in silica; and also used to encapsulate silica nanoparticles in titania [51].

### 1.3.2. Classification of reverse microemulsions.

K. C. Khilar et al [63] have classified reverse microemulsions into two classes: (a) the gas-liquid mode in which the nanoreactors are first formed with one of the reactants (in the liquid phase) already inside the reactors. Then a second reactant in the gas phase is passed into the system, dissolves in the continuous (oil) phase and diffuses into the micelles where the reaction takes place. (b ) The liquid-liquid mode which they further classified into the simple addition type involving the introduction of a liquid phase containing the reducing, oxidizing or precipitating agent to a microemulsion containing the other reactants, and the multiple microemulsion method which involves the mixing of more than one microemulsions containing different reactants. It should be noted that the microemulsion in the simple addition type of the liquid-liquid mode into which a liquid phase is added may not necessarily be a reverse microemulsion; in some cases, it is a microemulsion containing the continuous (oil) phase, surfactant, and every other reactant except water or the aqueous component. The water or aqueous phase (perhaps containing one or more reactants) is added at last to simultaneously form the nanoreactors and kick-start the reaction [57, 68, 72-73]; that is, as soon as the water or the aqueous phase is added, the nanopools enclosing the reactants are formed and the reaction takes off. One possible limitation here is that the nanopools may have a variation in the distribution of the reactants, a limitation that may be overcome by the concept of intermicellar exchange though, but as can be seen in the elaboration of the concept shortly, that may not be without its own setbacks. On the other hand, the simple addition method may involve firstly the formation of the nanoreactors with one or some of the reactants already enclosed before the second liquid phase containing another reactant(s) is added [31, 61, 71].

### 1.3.3. Factors affecting the use of the reverse micelle.

There are a number of factors reported in literature which affect the morphology, agglomeration and general stability of reverse micelles and the nanoparticles made in their interior. Zhang et al [71] reported that for a fixed R value, an increase in the average particles size of PbS nanocrystals was witnessed by increasing the solid loading of the $Pb^{2+}$ while X.

Fu and S. Qutubuddin [31] reported an increase in the size of silica nanoparticles with increasing amount of tetraethoxysilicate (tetraethoxysilane, silicon (IV) tetraethoxy, TEOS). The intermicellar electrostatic potential and the coulombic repulsion among the charged head groups of ionic surfactants are said to affect the size and stability (aggregation or not) of the micelles [69]. In a study on the coating of CdSe@ZnS core-shell nanocrystals with silica [57], a lot of interesting conclusions on the effect of the reaction parameters on size, size distribution, and agglomeration were arrived at. The authors concluded that:

1. At low surfactant (synperonic NP-5, an anionic surfactant) concentration, agglomerated silica particles were obtained, and with increasing surfactant concentration, first polydispersed and later monodispersed nanocrystals@silica nanoparticles were obtained. A later work on encapsulating $YF_3$ in silica using the same synperonic NP-5 corroborated the finding on the effect of surfactant on nanoparticles agglomeration [20]
2. Low concentration of the catalyst (aqueous ammonia) resulted in irregular silica particles while increasing concentration of ammonia led first to poly-dispersed nanoparticles with more than one nanocrystals in each and then to monodispersed silica nanoparticles with a single CdSe@ZnS nanocrystals. Increasing the concentration of the catalyst further led to irregular structures once more. Variation of the amount of TEOS gave a similar result. High amount of the nanocrystals also gave bigger nanoparticles
3. An increase in temperature, a little above room temperature, gave poly-dispersed and surprisingly, amorphous materials while good results were obtained at room temperature. High stirring rate was also reported as being superior to low stirring rate.

These results demonstrate the dynamics of the reverse micelle and the need for more studies on the system. The increase in particle sizes as a result of increasing amount of components can be pointers to the facts that the nanoreactors are not necessarily rigid reactors and may expand to accommodate more solid loading of reactants.

### 1.3.3.1. The concept of intermicellar exchange.

For the multiple microemulsion type of the liquid-liquid method and even the simple addition type which involves the addition of water or aqueous solution to the microemulsion (not reverse microemulsion) as the second liquid phase, intermicellar exchange, which is driven by uneven distribution of reactants in the micelles, is considered a pathway to nucleation and growth. It is also believed to be the major factor that determines the morphology of the particles formed in such systems and that effective Brownian collisions between micelles are the first steps towards its occurrence. There has not been much work or established theories on the concept but the general assumptions upon which existing models are based are that of (binary) collisions which leads to fusion of two micelles, subsequent exchange of their water contents, and finally, a fission process back to the original micelles [63-64, 68, 74], with the chances that only one of the micelles will inherit all the molecules while the other goes empty-handed [63]. The rate of effective collisions, that is collisions that are energetic enough to lead to fusion, therefore becomes the most important step in intermicellar exchange [72, 74]. The possibility of having varying number of molecules in the nanoreactors is still there even after the exchange process [64].

Bagwe and Khilar [72] studied the effect of intermicellar exchange on the formation of silver nanoparticles and also the factors affecting the process. Their conclusion on the effect of intermicellar exchange was that higher rate of intermicellar exchange was a result of high rate of collisions between micelles and that it leads to a large population of micelles with the reactants (as opposed to the reactants residing in a fewer number of micelles), and invariably smaller particles; and vice versa. They also found out that with increasing chain length of the oil phase, there was an increase in the rate of intermicellar exchange leading to smaller particles. The explanation for this was that increasing chain length meant increasing coiling of the chains and hence increasing difficulty in the penetration of the surfactants tail layer which translated to stronger intermicellar tail-tail interaction and therefore more collisions. Shorter chain length and acyclic oils easily penetrated the surfactant layer resulting in stronger interfacial rigidity. In addition, they reported that the addition of an effective co-surfactant- one whose molecules are smaller than those of the main AOT surfactant making it possible for its molecules not to be sterically hindered by the AOT- led to smaller particles.

In two different modelling studies of intermicellar exchange [63, 74], another dimension to the process was brought to the fore: intermicellar exchange is not limited to micelles with the reactants only but can also take place between micelles that have experienced nucleation, leading to three aspects of exchange:

1. The fusion between a nucleated micelle and a non-nucleated, reactants-containing micelle, leads to the transfer of the entire content of the latter to the former, leaving behind an empty micelle.
2. The fusion between two nucleated micelles, one containing a particle and the other liquid product molecules results in the transfer of the entire product molecules to the former.
3. The fusion of two micelles containing particles leads to the coagulation of the two particles to from a larger particle contained in one of the micelles.

From the foregoing on intermicellar exchange, it is safe to conclude that the concept has a significant effect on particle size and particle size distribution and that mastering and controlling it is important for a more effective and robust use of reverse micelles in producing nanoparticles.

## *1.4. Luminescence and bio (nano)technology.*

Light travels almost instantaneously and so has become one of the most reliable and convenient channels for transmitting signals. Since it can easily reach regions of complex and sensitive biomolecular systems (that are not accessible to other physical messengers), the use of luminescence spectroscopy to detect and quantify trace constituents in biological systems, environmental samples and even in food science and technology, has been on the rise in recent years. Besides, luminescence spectroscopy is highly sensitive, selective, non-destructive, and requires relatively inexpensive and rugged instrumentation [2, 75-77]. Therefore, luminescence spectroscopy has become more desirable for immuno assays, cellular imaging and monitoring of cellular processes than other processes such as the use of radioactive tags [75, 78]

### 1.4.1. Classes of luminescent tags in bioapplication.

#### 1.4.1.1. Organic dyes.

Among the earliest and most classical luminescent materials employed in bioassays are organic dyes such as rhodamine and fluoresceins. However, they have some shortcomings which include broad emission bands (which can pose a problem in multiplexing and sensitivity), short luminescence life times, small Stokes shift (difficulty in separating the excitation and emission signals), poor photochemical stability, and susceptibility to photobleaching [26, 78]. Although some new fluorescent dyes which are more resistant to photobleaching and insensitive to pH changes have come into spotlight in recent times, the problem of short life times and Stokes shift have not been satisfactorily overcome and so the search for more efficient luminescent probes has also focused on some other classes of materials [26]. Their setbacks notwithstanding, organic dyes are still popular because of their low cost, availability, and ease of usage [78].

#### 1.4.1.2. Semiconductor nanoparticles

Semiconductor nanoparticles, which are also referred to as quantum dots (QDs), are considered to be other promising luminescent tags for bioassays. They are reported to be several thousand times more stable against photobleaching, much brighter, and one-third less in spectral width than conventional organic dyes [62] , their spectral widths however are still much bigger than those of lanthanides. QDs have the unique property of emission wavelengths variation which is strongly size dependent- different colours spanning the entire visible/near infra red region can be got from the same materials by merely changing the size of the particles. This is a consequence of the so called quantum confinement effect, a confinement of the electron and hole wave functions in the nanocrystals when the size of the particles are reduced beyond the bulk-exciton Bohr radius, and consequently, an increase in the semiconductor band gap [79-80]. A combination of the broad absorption bands of QDs, narrow emission bands, and their size dependent emissions confer massive multiplexing bioassays capabilities on QDs and thus make them useful for the bioassays of cancer and

many other diseases which involve a lot of genes and proteins. In addition, their lifetimes (20-50 ns) are generally longer than that of organic dyes by one order of magnitude, and so QDs are highly considered as a new generation materials capable of bringing immense benefits to medical diagnosis [81].

However, there are a few limitations which QDs have to overcome in order to be the ideal candidates for bioassays, chief most among which is the danger of releasing toxic elements into biological systems, especially in in-vivo analyses (most of the optically efficient QDs are made up of one or more toxic elements such as cadmium and selenium) [82-83]. Another reported limitation of QDs is their tendency to suffer from optical blinking emission, a situation that is detrimental to real time assaying [78, 82]. Again, even though QDs are said to be more resistant to photobleaching than organic dyes, some studies [84-86] have reported various degrees of QDs fluorescence quenching under irradiation in ambient environment, with some of the authors [84-85] conclusively pointing to photo-oxidation of the nanocrystals as the cause. It is noteworthy that some of the QDs used in the studies on the effect of photo-oxidation on luminescence were the core-shell type, example CdSe@CdS dots. In these core-shell QDs, the inner semiconductor material (core) is give a protective layer (shell) in order to overcome the limitations to high luminescence yield of the core caused by surface [73] ; the shell is usually a wider band gap semiconductor. Apparently, it appears like photo-oxidation of QDs cannot be overcome by the core-shell approach. On the other hand, Wang et al [78], in a review of luminescent nanomaterials for biological labelling, reported that coating QDs with silica conferred improvement on their limitations without affecting their optical properties.

### 1.4.1.3. Lanthanide chelates (and time-resolved fluorescence)

In luminescence based bioassays, limits of detection and sensitivity are determined by the analyst ability to separate the signals coming from the analyte from background interferences emanating from Raman and Rayleigh scattering of the incident photon, emission from natural occurring phosphors in biological samples, and instrument optics; background interferences can greatly reduce the signal to noise ratio [10, 26 87-89] .Some background correction methods exist but they are not suited for assays in living tissues and are generally not very effective to

ensure high sensitivity in ultra-low concentrations of analytes [75]. Time-resolved fluorescence (TRF), which is more or less an exclusive preserve of lanthanides compounds, has become by far the most effective way of eliminating background interferences in order to enhance sensitivity [26, 35, 76, 88-89, 90-95]. This is made possible by the considerably long luminescence lifetimes of lanthanides which allows signals to be obtained well after all background interferences have ceased. The principle of TRF is illustrated in figure 1.7 and involves first an excitation of the system, cessation of the excitation which is accomplished by shuttering a continuous excitation source or by using a light source that can be extinguished rapidly, allowing enough decay time (during which the typical fluorescence from dyes and QDs would have decayed) for background interferences to leave the scene, and measuring the luminescence of the lanthanide [10].

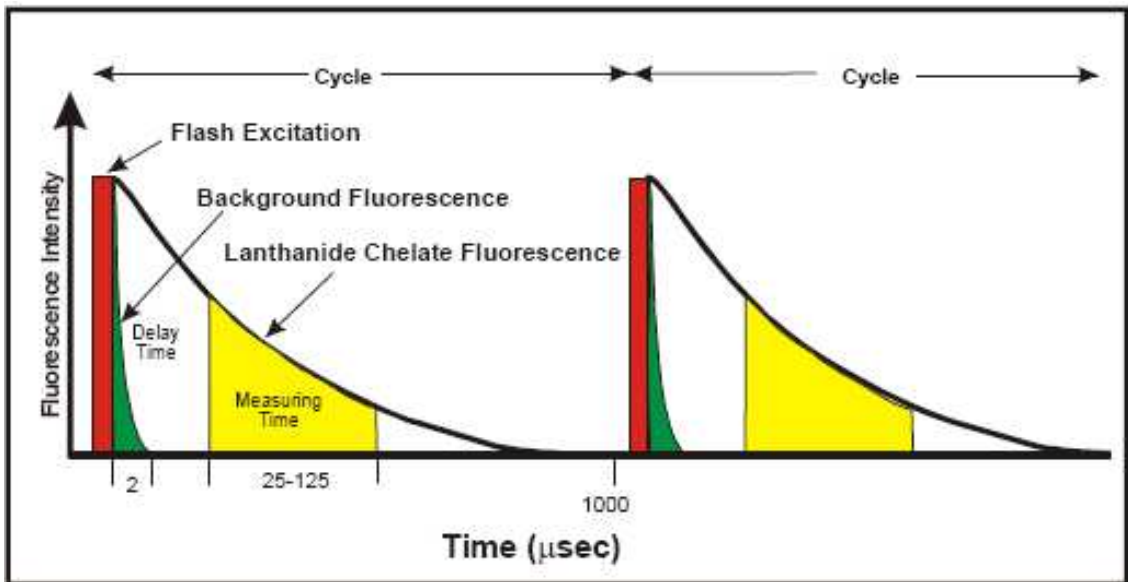


*Fig. 1.7: Principle of TRF. The excitation is removed, followed by a sufficient time delay, and later measurement of lanthanide fluorescence and the cycle can continue thereafter with new excitation.*

### 1.4.2. Lanthanides in heterogeneous bioassays.

Lanthanide chelates have been applied as luminescent probes in both heterogeneous and homogeneous environment, but especially the former due to its incorporation of a reliable assay performance occasioned by the removal of unbound labelled reagents. As such only bound labels which are immobilized on a solid support are detected or quantified. In a typical heterogeneous assay, a specific binding reagent (SBR), that is a molecule to which the analyte of interest can be attached to, is immobilized on a solid support, and the lanthanide chelate or enzyme (label) linked analyte is made to bind to the SBR, such that unbound labels and any other unwanted species can be washed off. The SBR could be an antibody, a nucleic acid or enzyme, depending on the type of bioassay [90].

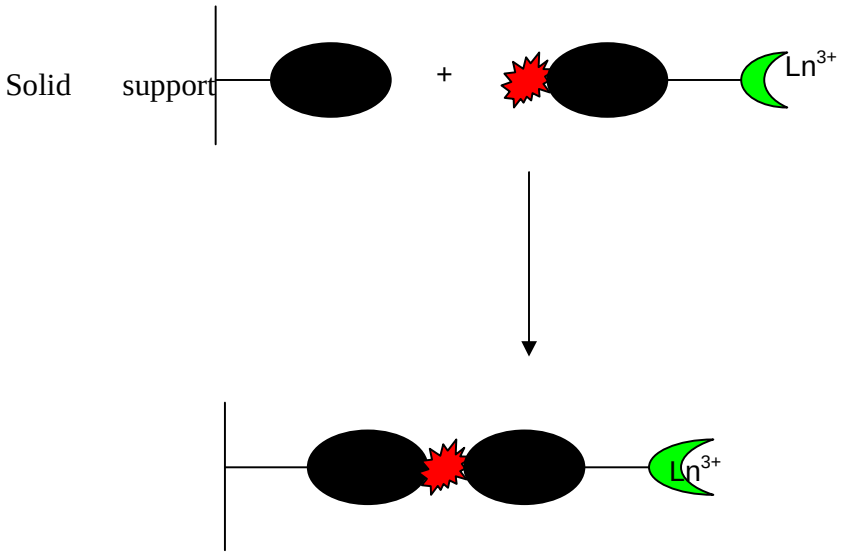


*Fig. 1.8: A heterogeneous assay: an SBR (black) is immobilized on a solid support and made to bind to the analyte linked to a lanthanide chelate by another SBR and then unbound labels/undesirable species are washed off.*

The three main aspects of lanthanide complexes heterogeneous systems include

1. Direct lanthanide chelate label-based luminescence assay (DLCLLA): In this procedure, the signal from the lanthanide complex is detected directly from the solid phase (e.g. electrophorectic gel, plastic microwell, microbead or membrane) and used to quantify the analyte [90, 92-93]. The requirements for such a system are that the lanthanide complex must be highly luminescent in water and chemically and photochemically stable (in order to be able to go through the different assay stages still intact). It is also important to select an appropriate solid support in order to minimize background interferences. An ideal lanthanide complex is not always readily available and this is often a limitation to the scope of application of this method [90]
2. Dissociation enhanced lanthanide fluoroimmunoassay (DELFIA): Here, after the washing off step, the lanthanide ions of the bound labels are dissociated to enter an

enhancement solution where they coordinate new ligands to become highly luminescent [76, 94, 96]; the initial lanthanide complex has little or no fluorescence and it is this separation of the binding and luminescence stages that have made this method the most widely used of the three.

3. Enzyme-amplified lanthanide luminescence (EALL). Here the label is not a lanthanide complex but an enzyme. After the washing off step, a substrate which the enzyme can act upon to give products that can form luminescent chelates with lanthanides is added [97]. Since an enzyme can act on different substrates to produce thousands of products, significant signal amplification can be realized and the scope of application of EALL can be widened.

### 1.4.3. Homogeneous bioassays-challenges and prospects.

For homogeneous bioassay, which is the realm where all in-vivo bioassays fall into, the requirements for a luminescent tags even become more stringent. Good sensitivity and selectivity are often more difficult to achieve than in heterogeneous assays [90] mostly due to absorption or scattering of the emitted signal by components in the system (especially for deep tissue in vivo assay) [81], the likely difficulty of separating the signal from bound labels from those of free labels (particularly for quantitative purposes) or other false positive events [98]. The problem of absorption or scattering of signals coming from the luminescent tags can easily be overcome by utilizing luminescent materials that emit in the NIR window where skin and tissue penetration is most effective [26, 81, 99]. In any case, development of a homogeneous assay method is highly desirable because of the need for simple assay protocols, instrumentation automation/miniaturisation, access to important biological kinetic data/processes through real time monitoring, higher throughput, and even circumventing the separation procedure which can be cumbersome in some cases [100-101].

More so, real time monitoring of cellular processes, even if they do not yield quantitative assays, are very important for *in vivo* or life cell studies in order to understand various hybridization events and changes that are sequel to genetic and malignant diseases [93, 101] ,

with the aim of drugs development or delivery or even targeting and killing tumours with NIR heat for example [99]. The four main techniques used for medical imaging are ultrasound imaging, computer x-ray tomography, positron emission tomography (using gamma rays), and magnetic image resonance (MRI) but they are not suited for detection of multiple markers and also do not posses high spatial resolution capable of detecting most of the very small early stage tumours; they are not the best for early detection of a disease like cancer which involves multiple cells and may become quite deadly by the time they have grown up to detection level. Optical imaging, especially luminescence imaging with nanosized probes, is considered a viable potential in this regard because of its intrinsic spatial resolution and multiplexing powers [81].

In order to separate signals from bound labels from other false signals in homogeneous assays, a number of luminescent probes have been developed, one of which is molecular beacons. Molecular beacons are oligonucleotide probes labelled with a reporter fluorophore at one end and a quencher at the other end. Their design is such that the luminescence of the fluorophore is quenched in the absence of hybridization with the complimentary target as a result of the close proximity of the quencher and fluorophore, while upon probe-target hybridization, the fluorophore is separated from the quencher and becomes luminescent. Although molecular beacons have improved specificity in comparison with linear oligonucleotide probes, they however can give false signals in vivo as a result of such factors as their degradation or opening by biomolecules: factors that lead to fluorescence in the absence of probe-target hybridization [98].

Jeng et al [102] have developed what could pass as sort of nanotube molecular beacons using the interaction between carbon nanotube (CNT) and DNA strands. They found that hybridization of DNA strands with their compliments which were already adsorbed onto the surface of the nanotube resulted in a red shift in the NIR luminescence of the CNT.

Another commonly used optical homogeneous assay method is Fluorescent resonance energy transfer (FRET). Here two SBRs are labelled, one with a donor and the other an acceptor, usually organic fluorophore. The principle is based on the transfer of absorbed energy from the donor to the acceptor when the two are in close proximity, the rate of energy transfer being dependent on the inverse sixth power of the distance between the donor and

acceptor. For most donor-acceptor pair, the distance corresponding to about 50% transfer efficiency is in the nanometre range and so FRET has become a unique method to probe the 1-7.5 nm range with about 0.1 nm resolution [100]. Since the signal wavelength is that of the acceptor, and not that of the excited donor, FRET is able to distinguish between target recognition from false signals because the energy transfer can only occur when the needed donor-acceptor distance is achieved by the bonding of the donor and acceptor to the same target [98]. In FRET, the lifetime of the acceptor contains a contribution from the lifetime of the donor, thus the use of lanthanide chelates as donors has made it possible to enhance the lifetime of organic fluorophore. As a result, distinguishing the signal from FRET from those of others, including that from non-FRET organic fluorophore can be realized by TRF [90, 100].

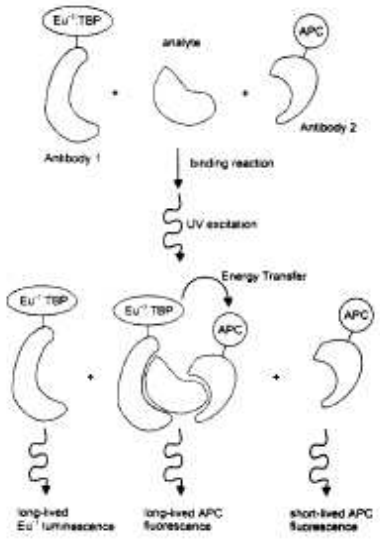


*Fig. 1.9: Schematic of FRET for a homogeneous assay [98]*

## *1.5. Why luminescent (silica/titania) nanoparticles?*

Nanotechnology is primarily concerned with the manipulation of materials and devices at the dimensions of nanometres with the aim of conferring on them some physical, chemical and biological properties which are either superior or complimentary to those of the conventional materials. For biomedical sciences and biotechnology, nanotechnology holds a lot of potentials in areas like drug delivery, gene delivery, and bioassays [62, 75, 81]. One obvious advantage of employing nanoparticles in bioapplication is that nanoparticles are within the dimension of biomolecules and cellular components and so can act as suitable probes and sensors [81, 103]. This is especially true for in vivo application where in addition to the nanoparticles providing a suitable surface for interacting with biomolecules, their small size becomes handy when they are injected into living tissues.

In the light of the superior potentials of optics (luminescence in particular) in bioapplication, its combination with nanotechnology will be of utmost importance for biomedical sciences and biotechnology. This is already being achieved with QDs and metallic (gold and silver) nanoparticles [104-105]. A way of transforming luminescent materials like organic dyes and lanthanide chelates into distinct nanoparticles that will become very pliable for bioapplication is encapsulating them in nanomatrixes, an approach that has also been extended to QDs as pointed out earlier. A number of luminescent materials have been housed in polymeric nanoparticles, namely: Eu:$Gd_2O_3$ nanoparticles@poly (L-lysine) nanoparticles [106], and Eu-complex@polystrene nanoparticles [91, 95]. The advantages of luminescent material-polymer nanocomposite include the enhancement of sensitivity due to the fact that several thousand luminescent centres are housed by the polymer, prevention of water-induced quenching of the luminescence of the lanthanides, and ease of conjugation of the polymer surface with almost all biomolecules [91]. However, polymers have some limitations in the high cost of their preparation, tendency to agglomerate in aqueous medium, swelling, which leads to leaking of the luminescent materials, and hydrophobicity [78, 106].

The inorganic nanomatrix overwhelmingly reported as being the most suitable for encapsulating luminescent materials for bioapplication is silica. As pointed out earlier, a

number of luminescent materials have been encapsulated in silica nanoparticles and the uses of such nanocomposite for a variety of bioapplications have been reported [62, 75, 78]. Silica is considered the best encapsulating matrix for both in vitro and in vivo bioapplication because of its good qualities (over organic materials) which include improved mechanical and chemical stability , non swelling in aqueous or organic solvent (hence the elimination of the leaching of the luminescent materials), non toxicity, very wide range of biomolecules that can be easily conjugated to it via functionalisation of its surface, optical transparency (which ensures it does not interfere with the absorption or emission of the luminescent centres), photostability even in oxygen rich environment, hydrophilicity, biological inertness, and the protection of the luminescent (nano)materials from the environment, including photoluminescence quenching as a result of oxidation [53, 57, 62, 65, 78, 82, 106-108]. Silica encapsulation has been reported to improve the photostability/photobleaching of organic dyes and lanthanide chelates [62, 78, 82, 109] as well as QDs [78]. The convenience offered by the ease of functionalisation and bioconjugation of the encapsulating silica matrix is especially good for lanthanide chelates and organic dyes, since one of the requirement for their use as biotags and which often places a limitation on their scope of usage, is that they should have a suitable functional group for bioconjugation [26, 62, 100]. A combination of the unique optical properties of lanthanide compounds with silica nanoparticles will therefore be ideal for the fabrication of biosensors and probes. Titania has also been indicated as a host matrix that can help eliminate the problems (already enumerated) associated with nanocrystals [73], and has also been reported as being biocompatible and optically transparent. Tan et al [110] reported the synthesis and biolabelling of Eu-chelate@silica@titania nanoparticles where the complex is covalently linked to the silica sub-backbone, but in general, titania, although widely studied, is lagging far behind silica in investigation of inorganic surfaces for biolabelling.

:

## *1.6. Aims of the research work.*

The objectives of the research project are as follows

1. To use reverse micelles to synthesize silica and titania nanoparticles that will house novel luminescent lanthanides complexes.
2. To investigate the photoluminescence of the as prepared nanocomposites.
3. To study the morphological characteristics of the nanocomposites by Transmission electron microscopy (TEM).

# Chapter 2. Silica encapsulation of lanthanide complexes

## *2.1. Synthesis*

3-hydroxypicolinic acid complexes of terbium (TbPic) and europium (EuPic) or the heterocomplexes containing the two lanthanides in the same molecule were encapsulated in silica nanomatrix via the reverse micelle method. Nanoencapsulation of picolinate complexes was discontinued because the resulting nanocomposites were no longer luminescent. For all nanocomposites series, the ratio of water to surfactant, R, was varied between 2 to 10. Details of all synthetic experimental procedures, including those of photoluminescence and transmission electron microscopy, are contained in chapter five.

The following observations were made during the synthesis of the silica-lanthanide complex nanocomposites (S-L):

1. The microemulsions generally remained transparent at the end of the experiment for lower R values (2 and 4), and upon the addition of acetone, especially for R = 2, the precipitates took some time before becoming noticeable such that it was possible to conclude that there was nothing in the reaction flask but for the aid of UV lamp. With increasing R values (6 to 10), the solution became increasingly cloudy such that at R values of 8 and 10, it was possible to notice precipitates descending to the bottom of the centrifuge tube even before the addition of acetone. The addition of acetone however was still necessary in order to precipitate out the nanoparticles completely.
2. After the precipitation step and when centrifuging was not done immediately, as was the case with most of the S-L samples, the samples of the lower R values (4 and 6 especially), settled at the very bottom of the centrifuge tube while those of 8 and 10 were not clearly at the bottom but rather floated on a small volume of solvent at the bottom of the tubes. In addition, higher R values gave bigger volumes of precipitates to work with unlike smaller R values, especially 2, which at times gave such small volumes of materials that almost got completely exhausted, during the washing process.

## *2.2. Photoluminescence.*

The photoluminescence excitation spectra of all the nanocomposites containing 3-hydroxypicolinate complexes of $Ln^{3+}$ and silica generally reveal that the ligand-lanthanide synergy is maintained after synthesis. The large ligand broad bands, in comparison with the peaks at 465, 526 and 535 nm representing direct Eu excitation for example, are a proof of the efficiency of the ligand (3-hydroxypicolinic acid) to absorb energy and transfer it to $Eu^{3+}$ ions even after the synthesis. However, there exist some degrees of variations, from each other and from the pure lanthanide complexes, in the various categories of nanocomposites made. This most likely means that the lanthanide environment was affected in diverse ways from one nanocomposite to the other, lanthanide ions being extremely sensitive to the environment. All PLE were monitored at 544 and 612 nm for $Tb^{3+}$ and $Eu^{3+}$ respectively, except otherwise indicated.

For all PL studies, there are little or no indication of emissions from the ligand in both the pure complexes and the nanocomposites. In general, the luminescence of $Tb^{3+}$ in both the pure complex and the composite materials is very poor and so the discussion will be focused mainly on $Eu^{3+}$.

### 2.2.1. Silica/Eu 3-hdroxypicolinic acid nanocomposite (S/EuPic)

The maximum PLE intensity positions of the different R values for the silica-EuPic nanocomposites (S/EuPic-2 to S/EuPic-10) show a disorderly variation from each other (363, 373, 368 and 380 nm for R = 2, 4, 6 and 10 respectively, see fig.2.1) This represents a blue shift of up to 15 nm from that of the pure Eu complex (378 nm) for the nanocomposites corresponding to R = 2. (R = 8 has been excluded for discussion in this series because of a contamination problem). As explained earlier, this trend shows the dynamic nature of the optical spectroscopy of lanthanide ions as they respond to their immediate environment, it also demonstrates a potential practical reality of using different excitation wavelengths on the same type of material in order to suit application or equipment needs.

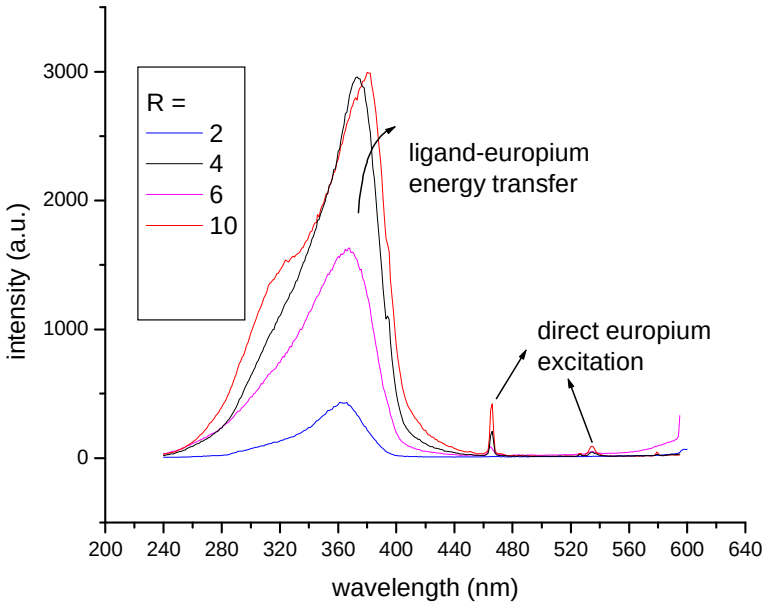


*Fig. 2.1. PLE of S/EuPic nanocmposites for distinct R values. Notice the shoulder around 320 mm in R = 10, the rest have a simple profile.*

The relative intensities of the direct europium excitation (at 465 nm)-relative to the highest peak of the ligand absorption (table 2.1)-also exhibit a disorderly variation pattern, with a value of 0.15 for EuPic complex, going down to 0.05 for R = 2 and up to 0.15 for R = 10. Note that the value of R = 10 is the same as that of the pure complex (EuPic), a situation that is almost akin to the maximum PLE intensity positions.

The PL features of the series as shown in table 2.1 and figures 2.2 (a-d) and 2.3 (a) show some variations among themselves but more importantly, from those of the pure Eu complex. The full width at half maximum (fwhm) of the $^5D_0 \rightarrow {}^7F_0$ transition of EuPic is 16.26 $cm^{-1}$ while those of the S/EuPic samples ranged from 24.14 (for R = 4) to 26.08 $cm^{-1}$ (for R = 10). This increase in fwhm values reveals an increased non-homogeneity for the $Eu^{3+}$ local coordination site [111]. Except for a very small decrease from 17248.57 for the pure complex to 17248.07 $cm^{-1}$ for R = 2, the energies of the $^5D_0 \rightarrow {}^7F_0$ lines increase for all members of the S/EuPic series, moving up to 17256.39 $cm^{-1}$ for R = 10. Changes in the $^5D_0 \rightarrow {}^7F_0$ energy are

highly dependent on the covalency (primary coordination sphere) of the $Eu^{3+}$. A red shift for the cation, with respect to the energy of the gaseous $Eu^{3+}$ (17374 $cm^{-1}$), means an increase in covalency [4, 111-112]. Thus, the blue-shift of the $^5D_0 \rightarrow {}^7F_0$ for the majority of the series members is an indication of a decreasing covalency of the $Eu^{3+}$ in the silica matrix. Goncalves et al [111] had attributed a blue shift in the energy of the $^5D_0 \rightarrow {}^7F_0$ for an ethanolic $Eu^{3+}$ sample to the incorporation of OH groups in the primary coordination sphere of the cation. The blue shift was with respect to the same $Eu^{3+}$ samples with their original Eu-O and Eu-N bonds and with no proximity to OH groups. The maximum splitting of the $^5D_0 \rightarrow {}^7F_1$ transition ($\Delta E\ ^5D_0 \rightarrow {}^7F_1$ in table 2.1) increases above the value for the pure complex for each nanocomposites in this series, with lower R composites having higher maximum splitting than higher R composites. This difference between the $\Delta E\ ^5D_0 \rightarrow {}^7F_1$ of the pure complex and those of the nanocomposites is also another confirmation of the alteration of the local environment of the $Eu^{3+}$. The magnitude of $\Delta E\ ^5D_0 \rightarrow {}^7F_1$ has been reported as being directly proportional to the strength of the ligand (crystal) field interaction [111]. The local field splitting of the $^5D_0 \rightarrow {}^7F_1$ and $^5D_0 \rightarrow {}^7F_2$ transitions into three and five stark components is more pronounced in the pure complex than in the S/EuPic series. The most intense emission peak, which belongs to the $^5D_0 \rightarrow {}^7F_2$ transition, shifts from 16267.89 $cm^{-1}$ (about 614.5 nm) in EuPic to between 16335.84 and 16342.53 $cm^{-1}$ (about 612 nm) in the S/EuPic series. In general, the number of Stark components detected for the $^5D_0 \rightarrow {}^7F_{1\text{-}4}$ transitions in both the pure complex and S/EuPic series indicate that the $Eu^{3+}$ ions occupy a low site symmetry while the high intensity of the $^5D_0 \rightarrow {}^7F_2$ transition is indicative of symmetry sites without inversion centres [4].

With R fixed at 10, and all other factors kept constant, the amount of EuPic added varied from 2 to 4 mg in one step increment (5mg of lanthanide complexes was used in all experiments except in this case and the series involving a mixture of EuPic and TbPic in which a total of 10 mg of combined lanthanide complexes were used). The fwhm,
$\Delta E\ ^5D_0 \rightarrow {}^7F_1$, and the energies of the $^5D_0 \rightarrow {}^7F_0$ transitions of the resulting composites, all varied slightly from the values of S/EuPic-10 (table 2.1). However, the luminescent features of the latter series still fall into the same class as those of the S/EuPic2-10.

Table 2.1.

| Name | FWHM ($cm^{-1}$) | $^5D_0$-$^7F_0$ $cm^{-1}$ | $\Delta E$ $^5D_0 \rightarrow {}^7F_1$ ($cm^{-1}$) | RELATIVE INTENSITY 465 nm | 535 nm |
|---|---|---|---|---|---|
| EuPic | 16.26 | 17248.57 | 208 | 0.15 | |
| S/EuPic-2 | 24.22 | 17248.07 | 270.1 | 0.06 | |
| S/EuPic-4 | 24.14 | 17250.68 | 271.92 | 0.07 | |
| S/EuPic-6 | 26.43 | 17249.12 | 257.3 | 0.05 | |
| S/EuPic-10 | 26.08 | 17256.39 | 257.82 | 0.15 | |
| S/EuPic-10,20 | 25.94 | 17249.12 | 244.41 | 0.03 | |
| S/EuPic-10,30 | 24.2 | 17249.93 | 255.25 | 0.06 | |
| S/EuPic-10,40 | 25.8 | 17254.02 | 258.64 | 0.04 | |
| S/Eu0.5 +Tb0.5-6 | 18.88 | 17258.96 | 348.98 | 0.23 | 0.06 |
| S/Eu0.5 +Tb0.5-8 | 17.72 | 17261.05 | 345.14 | 0.13 | 0.05 |
| S/Eu0.5+Tb0.5-10 | 18.42 | 17258.76 | 345.06 | 0.06 | 0.02 |
| S/Eu0.3+Tb0.7-6 | 18.2 | 17259.88 | 346.15 | 0.07 | 0.05 |
| S/Eu0.3+Tb0.7-8 | 17.33 | 17261.55 | 347.66 | 0.03 | 0.01 |
| S/Eu0.3+Tb0.7-10 | 18.18 | 17258.45 | 349.47 | 0.07 | |
| S/Eu0.1+Tb0.9-6 | 17.38 | 17258.94 | 346.5 | 0.02 | |
| S/Eu0.1+TB0.9-8 | 17.55 | 17256.36 | 345.16 | 0.02 | |
| S/Eu0.1+Tb0.9-10 | 18.28 | 17256.74 | 347.42 | | |

Owing to time constrain, time resolved luminescence was carried out only on representative samples of S/EuPic (R = 10) and T/EuPic (R = 10) composites as well as on EuPic itself to determine the life time, $\tau_{exp}$ , of the excited $^5D_0$ $Eu^{3+}$ energy level. The results show $\tau_{exp}$ of 0.431± 0.002 ms for EuPic and 0.45 ± 0.003 ms for S/EuPic. The efficiencies of the $^5D_0$ excited states are 24.8% and 10.3% for S/EuPic and EuPic respectively. This means that the radiative transition probability, $k_r$, of the $^5D_0$ excited state increases in S/EuPic relative to EuPic. Efficiency, $q$, is calculated as the ratio of the radiative to the sum of radiative and non-radiative transition probabilities of the $^5D_0$ $Eu^{3+}$ state, details of which is contained in chapter 5. An increase in $q$ and $\tau_{exp}$ for EuPic when embedded in a silica matrix (via a sol gel approach) over that of pure EuPic has been reported some where [4]; the results here corroborate that finding.

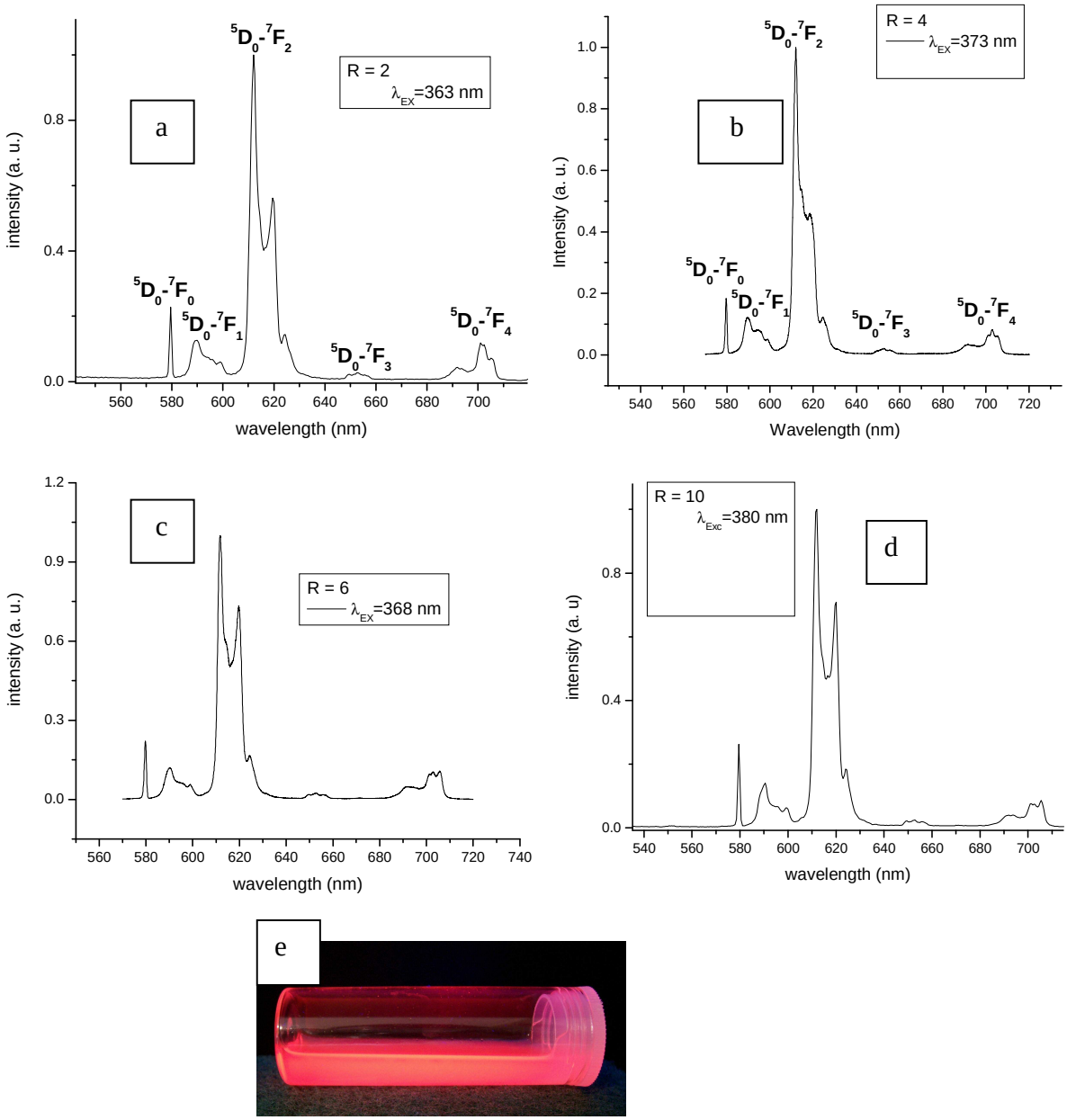


*Figs. 2.2 (a-d). PL spectra of S/EuPic from* ***a*** *(R = 2) to* ***d*** *(R = 10). Excitation was at the peak position of the excitation spectrum (indicated in each graph)*; (e) *photo of S/EuPic nanoparticles in 1-butanol.*

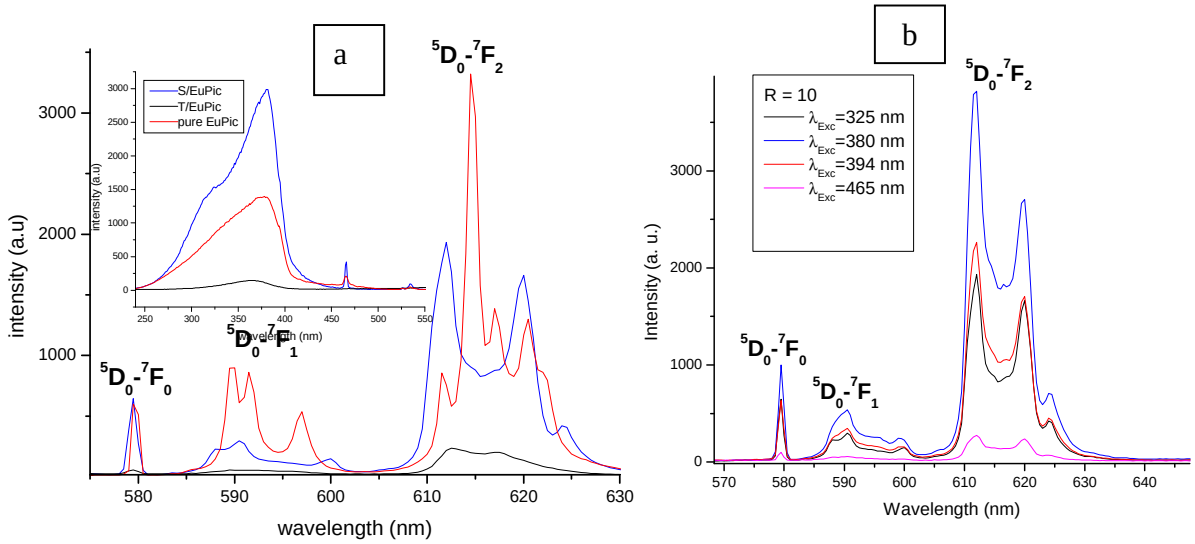


*Fig. 2.3: (a) PL of representative samples of S/EuPic (blue line) and T/EuPic (black line) and that of pure EuPic (red line). The inset shows the corresponding PLE spectra (colour labels the same). (b) PL spectra of S/EuPic-10 with excitations at different points on the PLE spectrum (325, 380, and 394 nm) and one at 465 nm. The oneness of all the resulting emission spectra is consistent in all the samples (pure complexes and composites) investigated in this work.*

### 2.2.2. Silica/(Eu-3hydroxypicolinate + Tb 3-hydroxypicolinate) nanocomposites (S/Eu+Tb).

With the Tb complex showing low luminosity, most of the optical investigation on this series of nanocomposites was again on $Eu^{3+}$. Just to see if the optical detection of $Tb^{3+}$ could be enhanced, the total amount of lanthanide complex was increased to 10 mg for each experiment starting with a 50:50 weight ratio between Tb and Eu complexes and increasing the ratio of the Tb complex in subsequent experiments (S/Eu0.5+Tb0.5-6 to S/Eu0.1+Tb0.9-10 in table 2.1) Even at a ratio of 90:10 in favour of the Tb complex, the luminescence of $Tb^{3+}$

was still very small and negligible in comparison to that of $Eu^{3+}$.

The $Eu^{3+}$ $^5D_0 \rightarrow {}^7F_0$ fwhm of the composites range from 17.33 to 18.88 $cm^{-1}$ (EuPic = 16.24 $cm^{-1}$), a good improvement over those of S/EuPic series. This indicates that the local coordination site of the $Eu^{3+}$ in the S/Eu+Tb series, in comparison to the pure complex, is fairly homogenous. The results also show that the $Eu^{3+}$ local environment suffered only a little alteration in this series than in the S/EuPic. A further proof to this is seen in their PL spectra which show a better detection of the Stark components of the $^5D_0 \rightarrow {}^7F_{1,2}$ transitions than in the other nanocomposite series, with the $^5D_0 \rightarrow {}^7F_1$ lines being very distinct (fig.2.5). This could mean that if the solid loading of EuPic in S/EuPic series was increased to say 10 mg or more, the fwhm and the Stark components of the resulting composites would improve. However, increasing solid loading will need to be balanced with maintaining good control over synthesis-product-particle morphology and size distribution, and the matrixes effectiveness in shielding the increased population of complexes. The energies of the $^5D_0 \rightarrow {}^7F_0$ transition increase slightly above those of S/EuPic. Just like in the S/EuPic series, there is a good consistency in the positions of the emission lines as seen in fig. 2.5, with the most intense line shifting to 620 nm (up from 612 nm for S/EuPic and 614.5 nm for EuPic).

The PLE excitation spectra (figs. 2.4 a-c) of the series also show some interesting points. S/Eu0.5+Tb0.5-6 and S/Eu0.5+Tb0.5-8 give spectra that are split into two crests, one centred around 322 nm and the other around 356 nm, while S/Eu0.5+Tb0.5-10 gives a simple profile peaking at 356 nm. With a ratio of 70:30 in favour of TbPic, only S/Eu0.3+Tb0.7-8 has a spectrum with two crests; S/Eu0.3+Tb0.7-6 has a profile peaking at 356nm, with a shoulder around 323nm, while S/Eu0.3+Tb0.7-10 still maintains a relatively simple profile with a peak at 358nm. When the ratio is 90:10, all R values give profiles with shoulders around 323 nm and peaks between 352 and 355 nm. An interesting observation here is that when the PLE spectra show two peaks, excitation at the lower one (in terms of wavelength value) gives a more intense emission than the upper one while the profiles with a simple profile or shoulders give more intense emission on excitation at the peak spectra position.

The relative intensities of the 465 nm direct Eu excitation generally decrease as the Tb:Eu ratio increases, ranging from 0.23 for S/Eu0.5+Tb0.5-6 to 0.02 for S/Eu0.1+Tb0.9-6 and S/Eu0.1+Tb0.9-8; there is no observation of any direct excitation for S/Eu0.3+Tb0.7-10. In

addition, there is a significant presence of another direct Eu excitation at 535 nm, except for the samples with Tb:Eu ratio of 90:10.

Excitation at 544 nm (for Tb) does not yield any significant result except for the 90.10 samples, but all the samples in this series, except S/Eu0.5+Tb0.5-6 and S/Eu0.5+Tb0.5-8, show the Tb luminescence; the 90:10 ratio samples being more significant (table 2.2). The $Tb^{3+}$ PLE profiles of S/Eu0.1+Tb0.9-6 and S/Eu0.1+Tb0.9-8 (fig. 2.4 d) bear a resemblance to those of $Eu^{3+}$ in the series: S/Eu0.1+Tb0.9-6 has a peak at 354 nm with a shoulder around 321 nm and S/Eu0.1+Tb0.9-8 has two peaks at 322 nm and 352 nm. This resemblance factor could mean that the absorption of photon by the ligand in the absence of coordination to lanthanide ions is also vulnerable to change under the synthetic conditions used in this work.

Table 2.2

| Name | Tb: Eu | R | $\lambda_{Ex}$ producing most intense Eu emission line | Relative intensity* |
|---|---|---|---|---|
| S/Eu0.5 +Tb0.5-6 | 50:50 | 6 | 323 | - |
| S/Eu0.5 +Tb0.5-8 | ″ | 8 | 321 | - |
| S/Eu0.5+Tb0.5-10 | ″ | 10 | 356 | 0.02 |
| S/Eu0.3+Tb0.7-6 | 70:30 | 6 | 356 | 0.02 |
| S/Eu0.3+Tb0.7-8 | ″ | 8 | 325 | 0.01 |
| S/Eu0.3+Tb0.7-10 | ″ | 10 | 358 | 0.02 |
| S/Eu0.1+Tb0.9-6 | 90:10 | 6 | 355 | 0.06 |
| S/Eu0.1+TB0.9-8 | ″ | 8 | 352 | 0.06 |
| S/Eu0.1+Tb0.9-10 | ″ | 10 | 352 | 0.05 |

* *Relative intensity of the 542 nm Tb emission to the 620 nm Eu emission*

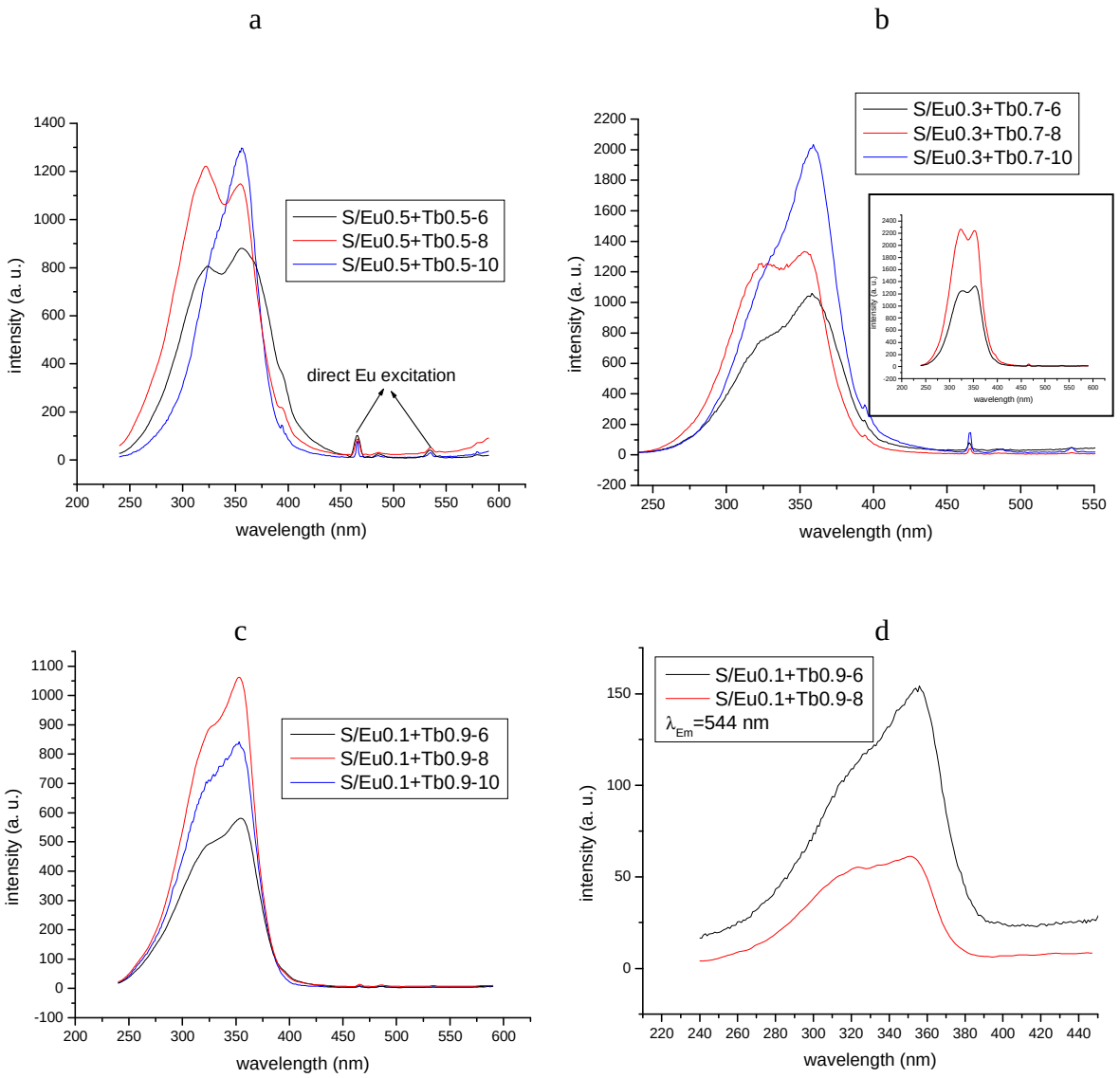


*Figs. 2.4: (a-c) PLE of $Eu^{3+}$ in S/Eu+Tb nanocomposites. The inset of **b** shows the relative intensity of S/Eu0.3+Tb0.7-8 when emission was collected at 612 nm (black line) and 620 nm (red line); notice the change in the relative heights of the two crests from the former to the later. (d) PLE of $Tb^{3+}$ in S/Eu+Tb, the profiles are roughly in the wavelength range of the $Eu^{3+}$ spectra.*

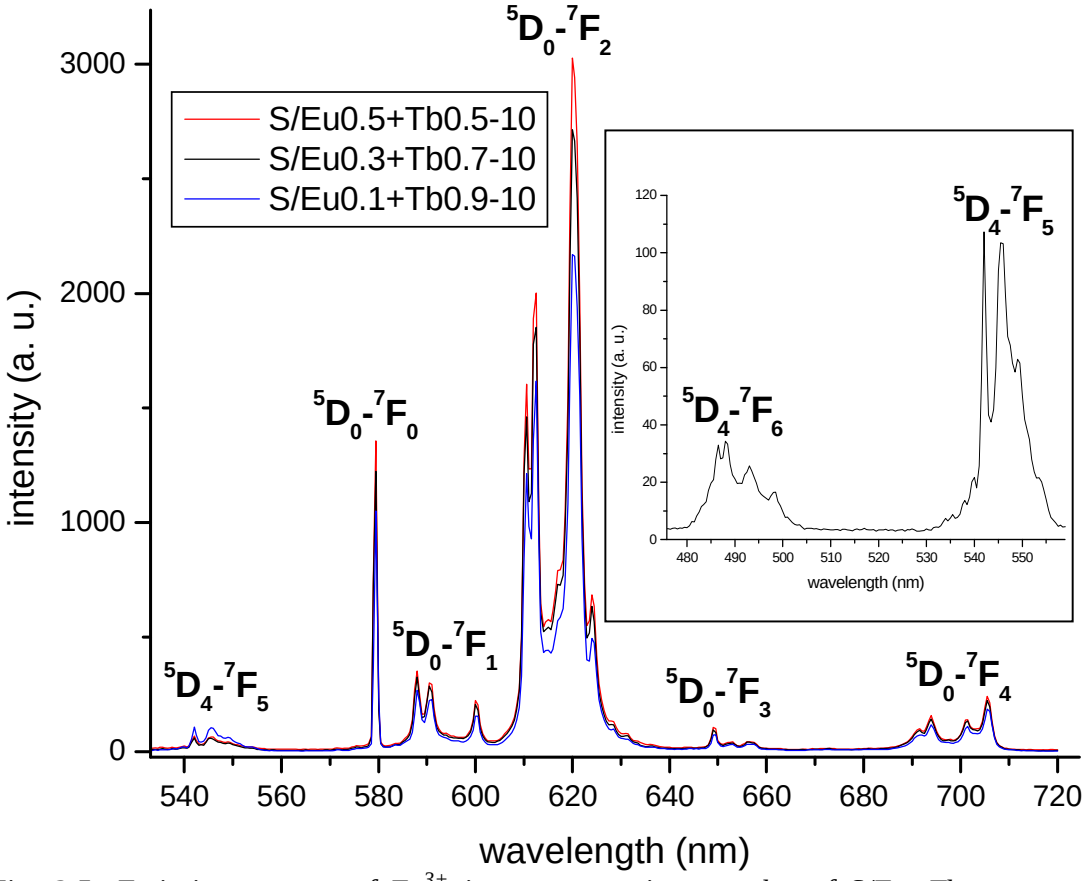


*Fig. 2.5: Emission spectra of $Eu^{3+}$ in representative samples of S/Eu+Tb nanocomposite series. Again, there is consistency of profile in all the samples and in different excitation wavelengths for the same sample; the $^5D_4 \rightarrow {}^7F_5$ transition comes from $Tb^{3+}$. The inset shows the emission of $Tb^{3+}$ from S/Eu0.1+Tb0.9-10, the same profile is seen for all relevant samples regardless of whether it is obtained by running emission spectrum for $Tb^{3+}$ alone or extracted from the emission spectrum run for $Eu^{3+}$.*

### 2.2.3. Silica/3-hydroxypicolinate heterocomplexes of Eu and Tb (S/Eu)

The heterocomplexes were prepared in order to investigate the effect of the presence one lanthanide on the luminescence of the other lanthanide, specifically, to access the possibility of obtaining the lanthanide-lanthanide synergy. Besides, the possibility of tuning the $Eu^{3+}$ emission was borne in mind in the preparation of the heterocomplexes. Table 2.3 is a summary of luminescent data for the heterocomplexes themselves and their composites with silica. Again, due to the poor luminosity of the $Tb^{3+}$ ions in the heterocomplexes, the remainder of the discussion, except for some passing remarks on $Tb^{3+}$, will be concentrated on $Eu^{3+}$. The Eu:Tb ratios reported here are all theoretical.

Table 2.3

| Name | FWHM ($cm^{-1}$) | $^5D_0 \rightarrow {}^7F_0$ ($cm^{-1}$) | $\Delta E\ ^5D_0 \rightarrow {}^7F_1$ ($cm^{-1}$) | RELATIVE INTENSITY. 465 nm |
|---|---|---|---|---|
| 0.5Eu | 18.09 | 17258.98 | 324 | 0.08 |
| 0.3Eu | 17.96 | 17254.48 | 327.91 | 0.05 |
| 0.1Eu | 17.72 | 17255.72 | 323.16 | 0.03 |
| S/0.5Eu-8 | 25.11 | 17248.8 | 250.29 | 0.04 |
| S/0.5Eu-10 | 24.51 | 17250.23 | 254.85 | |
| S/0.3Eu-8 | 24.79 | 17245.12 | 248.11 | 0.02 |
| S/0.3Eu-10 | 24.24 | 17246.83 | 249.47 | 0.02 |
| S/0.1Eu-8 | 29.36 | 17244.22 | 241.13 | 0.01 |
| S/0.1Eu-10 | 27.85 | 17248.08 | 250.16 | 0.03 |

PLE spectra for $Eu^{3+}$ on the three heterocomplexes (fig. 2.6 a) show a roughly good similarity, all peaking at 357 nm, with 0.5Eu revealing another peak or shoulder around 330 nm. The relative intensity of the 465 nm direct europium excitation decreases as the ratio of $Eu^{3+}$ decreases (increasing $Tb^{3+}$ concentration), ranging from 0.08 for 0.5Eu to 0.05 for 0.3Eu and to 0.03 for 0.1Eu; in contrast to the 0.15 value of pure EuPic. This could pass for an initial suspicion of the presence of energy transfer from the ETS of $Tb^{3+}$ to that of $Eu^{3+}$, considering the fact that $Tb^{3+}$ has got no emission line at 612 nm

where emission was monitored. Moreover, the luminescence of $Tb^{3+}$ in the heterocomplexes is very poor, such that the usually most intense $Tb^{3+}$ emission line at 542 nm only becomes significantly noticeable in 0.1Eu.

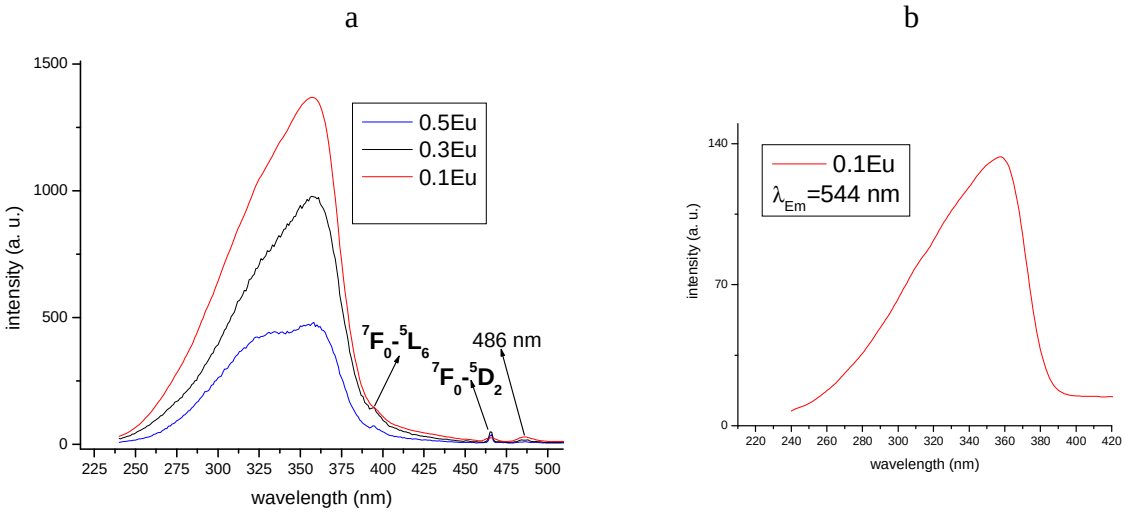


*Figs. 2.6. (a) PLE spectra of $Eu^{3+}$ in heterocomplexes;(b) PLE spectrum of $Tb^{3+}$ in 0.1Eu*

An even stronger suspicion of Tb-Eu synergy is seen in a small absorption band located at 486 nm (20, 576.13 $cm^{-1}$). There is neither a direct Eu excitation nor a ligand absorption that matches that wavelength in this work nor in literature. On the contrary, the absorption (at 486 nm) can be assigned to the $^7F_6 \rightarrow {}^5D_4$ direct Tb excitation [2]. Furthermore, the PLE of S/TbPic nanocomposites (fig. 2.9 d) also reveal clearly the absorption at 486 nm, which makes it more likely that there is a transfer of energy from Tb to Eu in the heterocomplexes. An energy dispersive x-ray spectroscopy (EDS) analysis on a 0.1Eu nanocomposite shows a significant presence of Tb and none of Eu (section 4.4 and fig. 4.6 in the next chapter); it is noteworthy that even at this mole ratio (0.9:0.1 in favour of $Tb^{3+}$ ), the complex still shows a strong $Eu^{3+}$ emission. As is the case with the mixed complexes based nanocomposites, PLE spectra for

$Tb^{3+}$ in 0.1Eu shows a profile similar to that of $Eu^{3+}$, with a peak at 357 nm (fig. 2.6 b). The $Eu^{3+}$ emission spectra of the heterocomplexes (fig. 2.7), apart from being uniform, reveal a good detection of the stark components of the various transitions, with the $^5D_0 \rightarrow {}^7F_2$ transitions showing only four out of the five Stark components, unlike the pure EuPic which shows all five components. The fwhm decreases with decreasing $Eu^{3+}$ concentration, from 18.09 $cm^{-1}$ for 0.5Eu to 17.72 $cm^{-1}$ for 0.1Eu (that of EuPic is 16.26 $cm^{-1}$). Again, just as in the composites formed between silica and mixtures of TbPic and EuPic, their most intense emission line is located at 620 nm, up from 612 nm for S/EuPic and 614.5 nm for EuPic; while the energies of the $^5D_0 \rightarrow {}^7F_0$ transitions increase slightly above that of EuPic. The $\Delta E$ $^5D_0 \rightarrow {}^7F_I$ of the heterocomplexes increase well above the 208 $cm^{-1}$ value for EuPic, ranging from 323.16 $cm^{-1}$ for 0.1Eu to 327.91 $cm^{-1}$ for 0.3 Eu. This shows a stronger ligand field interaction in the heterocomplexes than in EuPic. It can therefore be seen from the foregoing that the presence of $Tb^{3+}$ ions in the heterocomplexes affects the local coordination of $Eu^{3+}$ ions and hence their optical features. In order to understand the effects of $Tb^{3+}$ ions on the optical features of $Eu^{3+}$ better, more experimental work, including elemental analysis on the heterocomplexes to determine the actual ratio of Tb to Eu, need to be carried out.

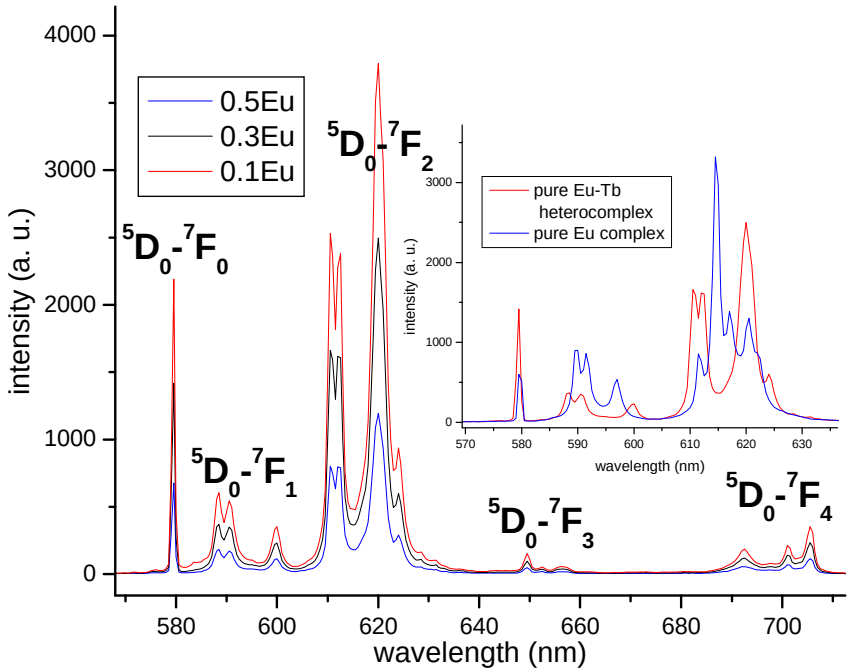


*Fig. 2.7: PL of $Eu^{3+}$ in heterocomplexes. The inset shows a comparison between the PL of $Eu^{3+}$ in heterocomplex (red) and EuPic (blue)*

It can be clearly seen that the optical features of $Eu^{3+}$ in the nanocomposites formed between the heterocomplexes and silica once more are vulnerable to changes when embedded in a silica matrix via the synthetic strategy employed in this work. The PLE spectra of the composites (figures not shown) roughly approximate those of the pure complexes, their peaks ranging from 355 nm to 357 nm, except for S/0.1Eu-10 which peaks at 362 nm, and S/0.5Eu-10 with a peak at a distant 370 nm. The two-crested profile of 0.1Eu is not seen in its composites, while the relative intensity of the 465 nm absorption in the excitation spectrum decrease from the values of the heterocomplexes, 0.5Eu experiencing the greatest dip.

Quite a few interesting changes are witnessed in the photoluminescence of the composites. The fwhm (table 2.3) of $^5D_0 \rightarrow {}^7F_0$ transitions increase significantly, ranging from 24.24 $cm^{-1}$ for S/0.3Eu-10 to 29.36 $cm^{-1}$ for S/0.1Eu-8, with the composites of 0.1Eu showing higher

values than the rest. Generally, the R = 8 composite of each heterocomplex shows a higher fwhm value than the R = 10 counterpart. As manifested in the energies of the $^5D_0 \rightarrow ^7F_0$ transitions which decrease slightly from those of the pure heterocomplexes, the Eu3+ ions in the nanocomposites experience some increase in covalency. The $\Delta E$ $^5D_0 \rightarrow ^7F_I$ of the nanocomposites decrease significantly from the values for the pure heterocomplexes; the range of the decrease is from 69.15 $cm^{-1}$ for 0.5Eu to 82.03 $cm^{-1}$ for 0.1Eu . There is again a general uniformity in PL spectra (fig. 2. 8) of all the composites, their most intense emission line shifting from 620 nm for the pure complexes to 611.5 nm, except for a small red shift of 0.2 and 0.4 nm for S/0-1Eu-8 and S/0.1Eu-10 respectively. The number of Stark components detected for the $^5D_0$-$^7F_{1,2}$ transitions is each short of one but generally remains good.

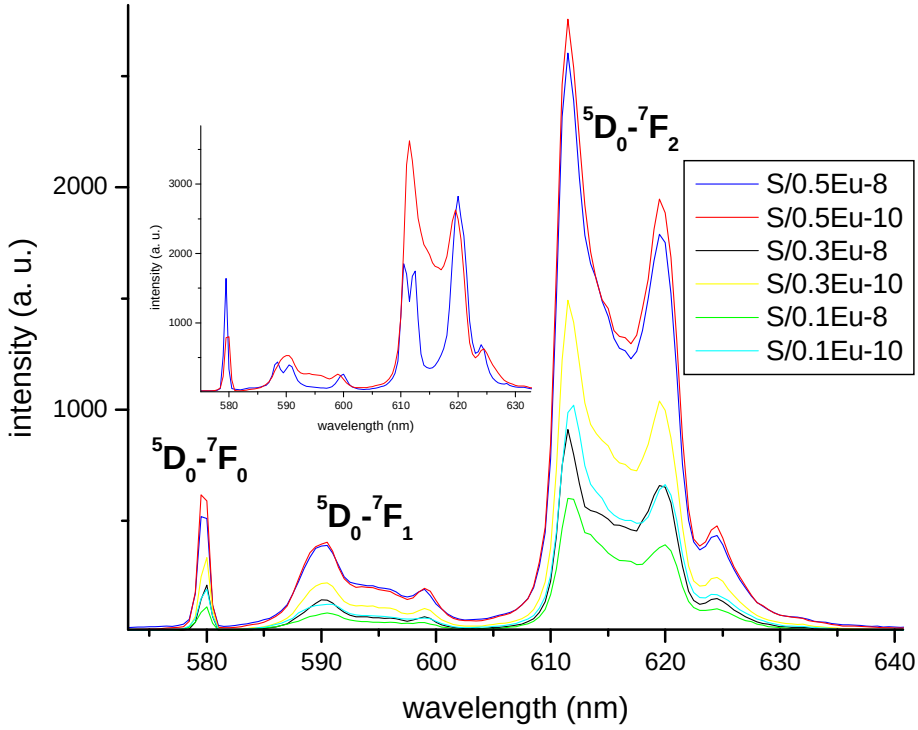


*Fig. 2.8: $Eu^{3+}$ PL spectra of heterocomplexes based nanocomposites. The inset shows a comparison between them and the pure heterocomplexes.*

### 2.2.4. Silica/Tb 3-hydroxypicolinate nanocomposites (S/TbPic)

Even though the optical features of 3-hydroxypicolinate complex of $Tb^{3+}$ are not of much interest in this work, a little interesting development made it imperative to cast a quick glance at the S/TbPic series in this subheading. It was not possible to detect any optical signal from the lower R values of the series and even from the pure TbPic itself both under the UV light and in the equipment used in monitoring PLE and PL in this studies; the same equipment that was adjusted severally during the studies on $Eu^{3+}$ because of over-ranged signals. The case of TbPic is even more intriguing because initially, the complex showed some green emission under the UV light which seemed to have vanished after some time (a period of about three months); besides, there was more than enough quantity of TbPic to play around with in order to squeeze out some amount of signal from it. The composites of the R values from 6 to 10 yielded some (even though very small) signals that were detected, with R = 10 giving off a faint green emission under the UV light. The questions that arise are: 1. did the TbPic complex undergo a sort of change or decomposition that destroyed whatever little luminescence it had, a change that was spared the encapsulated complexes? 2. Is it that the synthetic step and/or the encapsulation at higher R values enhanced the luminescence of the $Tb^{3+}$? Note that the luminescence studies on the TbPic and S/TbPic series were done around the same time. This development could be a mere accident that does not hold any scientific value but it could also be a pointer to something that is scientifically relevant.

The PLE spectra of S/TbPic-6 to S/TbPic-10 (fig 2.9 d), show similar profiles that are double-crested with the first peak around 320 nm and the second at 353 nm. For R = 6 and 8, excitation on the first peak wavelength give the most intense emission while for R = 10, it is excitation at the second peak wavelength of 353 nm that gave the most intense emission. On a closer look, there appears to be no well defined valley between the two peaks in R = 10, and so the profile may be considered as approximately a single-peak one with a shoulder at 320 nm. If this assumption holds, then the photoluminescent behaviour of $Tb^{3+}$ in S/TbPic-10 and the entire series in general can be considered to be similar to that of $Eu^{3+}$ in the series of nanocomposites containing a mixture of EuPic and TbPic. It should also be noted here that in the composites of mixed complexes, the R = 10 composites of the various mixture ratios tend more to having simpler PLE excitation profile than the R = 6 and 8 composites. The band at

486 nm is a direct $^7F_6 \rightarrow {}^5D_4$ Tb excitation. There is here also a good uniformity in the PL spectra of the composites, their most intense line located at approximately 542 nm, with the number of Stark components detected being also good.

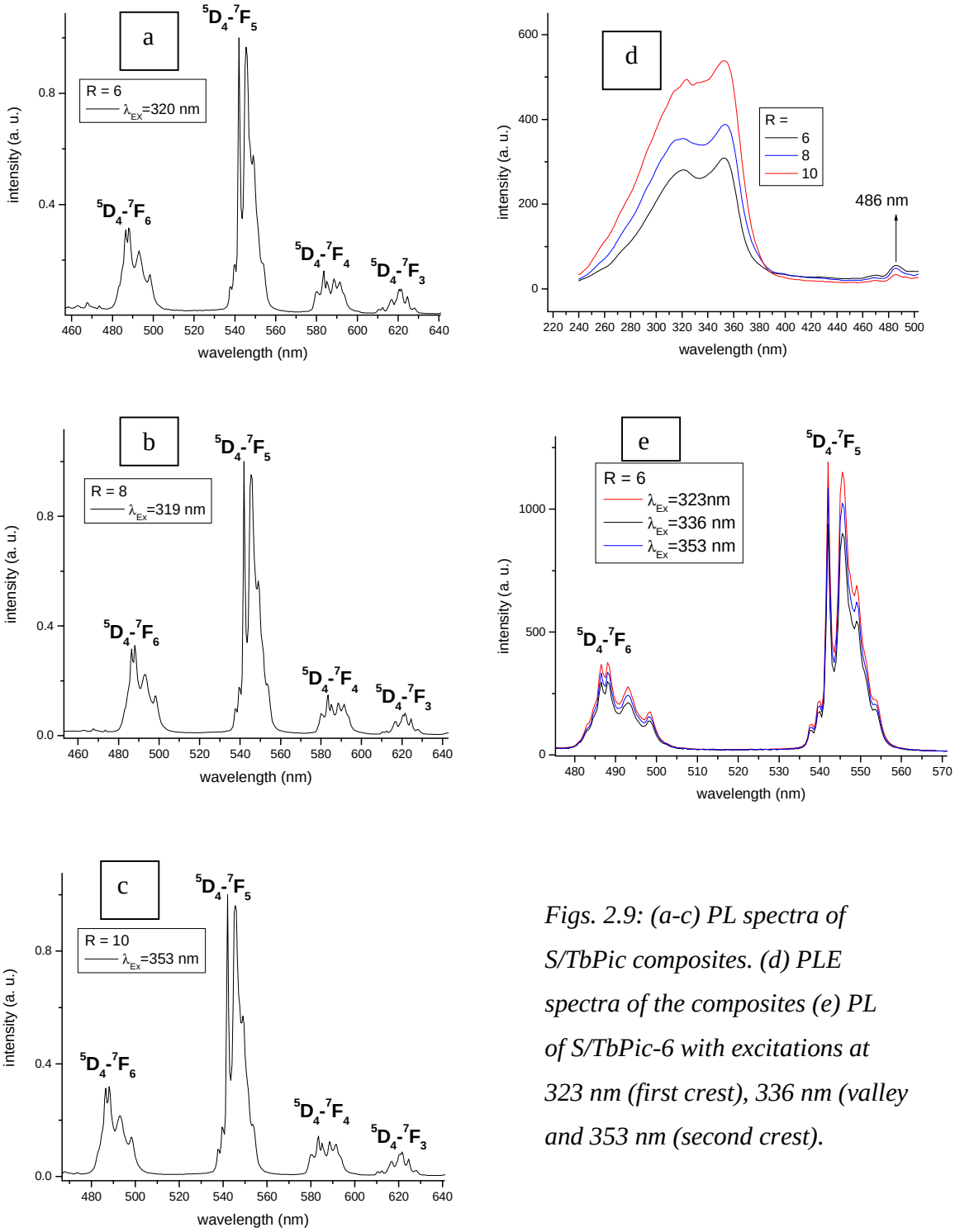


*Figs. 2.9: (a-c) PL spectra of S/TbPic composites. (d) PLE spectra of the composites (e) PL of S/TbPic-6 with excitations at 323 nm (first crest), 336 nm (valley and 353 nm (second crest).*

## *2.3. Transmission electron microscopy (TEM).*

The main objectives of the TEM studies are to determine the morphology and size distribution of the nanocomposites and hence correlate them to the synthetic strategies. It is also important to determine if the nanoparticles are distinct or agglomerated, because that will determine their suitability or versatility for bioapplication: For instance, agglomerated particles are not desirable because they will present less surface area for bioconjugation and will be difficult to use in vivo due to size restriction and unsuitability for single molecule/cell targeting. Of interest in the TEM studies is to confirm if the size of the nanoparticles in a series will increase as the R value increases, a common phenomenon with reverse microemulsion. The samples studied included the entire S/EuPic series and selected samples from the composites of heterostructures with silica, and those of mixed complexes with silica. Energy dispersive x-ray analysis (EDS) was employed to probe the presence of elements of interest in the nanoparticles.

The TEM studies were not really easy owing partially to the difficulty experienced in dispersing the particles in solvent and dimness of some particles on the carbon coated copper grid. The TEM studies were done some 2-3 months after the synthesis and luminescent studies, at a time when virtually all the samples were completely dries despite the efforts made to keep them in solution. Therefore, and for the sake of simplicity, average size estimates will be limited to the S/EuPic series (table 4.1), which were studied in more details; the other particles studied will be considered in the next subheading (S/0.1Eu-10, from the heterocomplexes based composites, is a particularly interesting case study).

Unfortunately, TEM images can not reveal the distribution of the lanthanide complexes in the nanoparticles-whether they have a preference to stay in the centre of the particles for example: The lanthanide molecules are not electron-dense enough to offer the possibility of detecting them in contrast to the silica matrix.

### 2.3.1. TEM of S/EuPic composites

Table 2.4 gives a summary of the average particle size (APS) and particle size range (PSR) of each composite as determined from the TEM images. The term PSR and not standard deviation is used here to give a rough idea of the particle size distribution because some images do not have enough clearly seen particles to allow for a uniform statistical calculation. Where there is a strong suspicion of inter-particle fusion to form very large particles with the sample showing a preponderance of much smaller particles that are within a close size distribution, the average size of the latter is considered the authentic APS for the sample. The unusually large particles will be discussed later.

Table 2.4

| Name | Average particle size, APS (nm) | Particle size range, PSR (nm) |
|---|---|---|
| S/EuPic-2 | 12 | 7-15 |
| S/EuPic-4 | 31 | 28-33 |
| S/EuPic-6 | 38 | 27-44 |
| S/EuPic-8 | 43 | - |
| S/EuPic-10 | 56 | 30-78 |
| S/EuPic-4’ | 29 | 25-36 |
| S/EuPic-8’ | 62 | 38-78 |
| S/EuPic-10’ | 77 | - |

In agreement with literature, the APS of the S/EuPic composites increase with increasing R value. The PSR shows very high size distribution at higher R values; EuPic-4 has the narrowest size distribution. The average particle sizes of the S/EuPic’ composites (prepared by adding aqueous ammonia before TEOS) not only increase with increasing R value, but it

is also found that R = 4 gives a good size distribution. This can be taken to mean that R = 4 is suitable for producing better monodispersed particles under the synthetic conditions/parameters used. Generally, the particles are spherical, and roughly not agglomerated (except for what very much looks like superimposition of particles on each other which most likely occurred during TEM sample preparation)

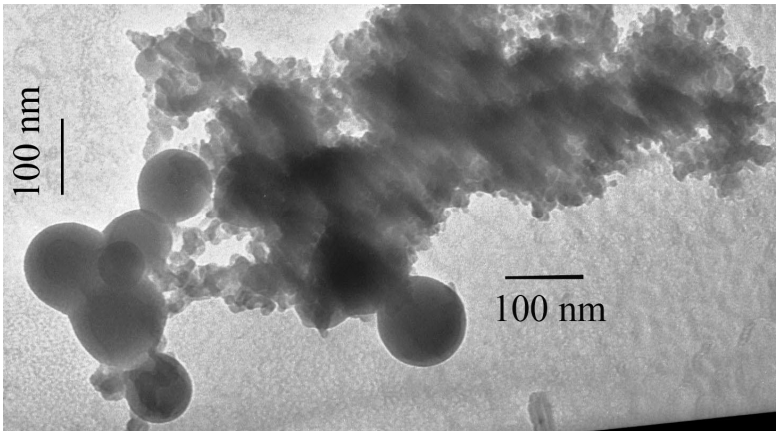


*Fig. 2.10. TEM image of S/EuPic-2*

It can be seen that S/EuPic-2 has a few very large particles (about 10) in the midst of thousands of very much smaller ones, a development that is not seen in others. This may be considered to arise from inter-particle fusion. The large particles appear to exist in 3 size ranges of 60, 97, and 120 nm. Since it was not possible to get other particle clusters (R = 2 composites were especially difficult to handle) in order to ascertain if the presence of the few large particles was common to S/EuPic-2, it will not be possible to make further conclusion on this phenomenally large few particles among a multitude of other much smaller ones.

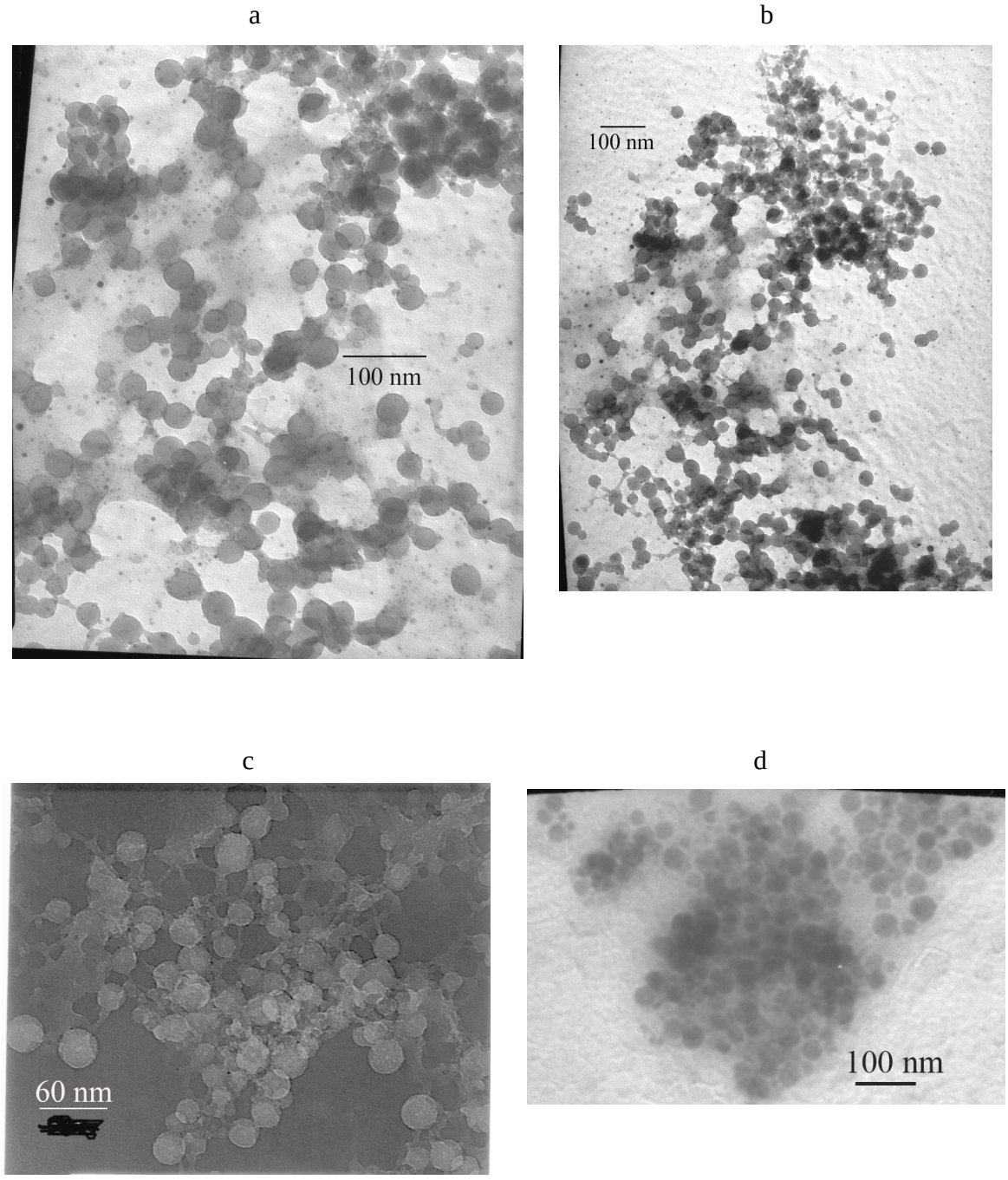


*Figs. 2.11. TEM images of: (a & b) S/EuPic-4; (c) S/EuPic-4'; (d) S/EuPic-6. The dark images in* ***a*** *and* ***b*** *are a result of superimposition of particles.*

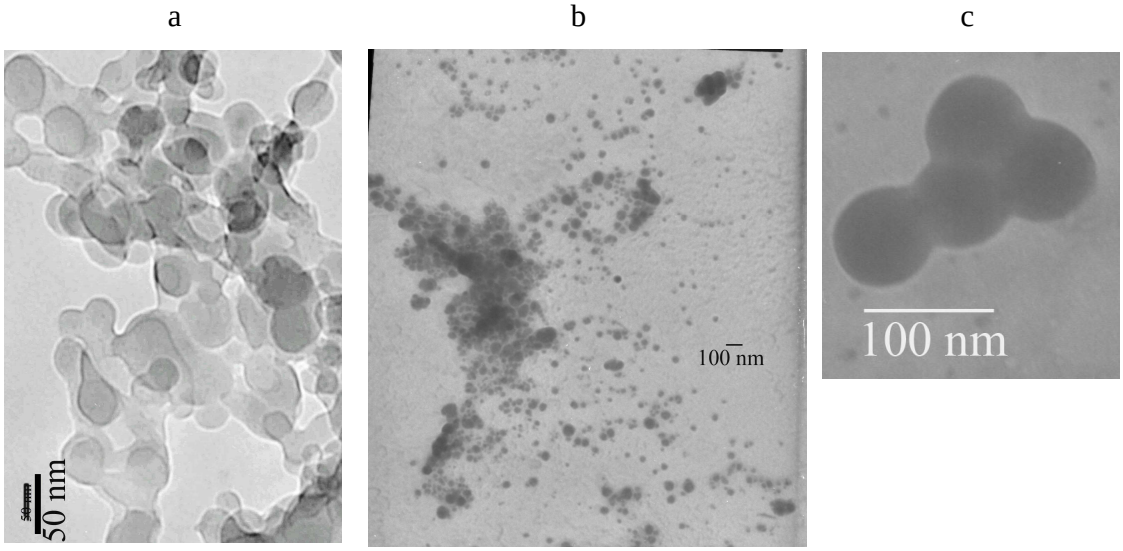


*Figs. 2.12. TEM images of: (a) S/EuPic-8; (b) S/EuPic-10; (c) S/EuPic-10´*

As stated earlier during the literature review, factors like the amount of solid loading and the quantity of catalyst can affect the morphology and size distribution of the particles obtained in a typical reverse micelle experiment. The wide particle size distribution at higher R values and even the presence of the large particles in S/EuPic-2 can be rationalized on the basis of high or low ammonia concentration as, for example, R= 2 (50µl of water) is 400% more ammonia concentrated than R = 10 (245 µl of water). Furthermore, TEM results of a nanocomposite containing silica and 2, 6-dihydroxybenzoate complex of $Eu^{3+}$, S/EuDhb-4 (figure 2.13), which was prepared under the same condition as the S/EuPic series but with lower solid loadings of 3 mg of complex and 80 µl of TEOS, and lower ammonia concentration of 55 µl, shows particles that are 6-9 nm in size and somewhat elongated. This is a clear deviation from S/EuPic-4 particles. The S/EuDhb series was discontinued because of poor luminescence and the parameters adjusted in subsequent series to match more findings from literature.

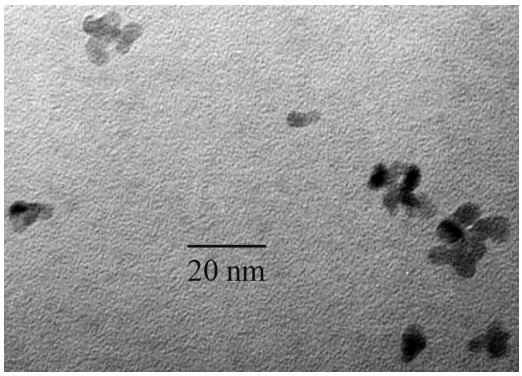


*Fig. 2.13. TEM image of S/EuDhb-4, Dhb = 2, 6 dihydroxybenzoate.*

EDS analyses on all the samples reveal the presence of silicon and europium. Europium was hardly detected when the analyses was done on single particles which is normal, considering that the $Eu^{3+}$ ions should be in a small amount.

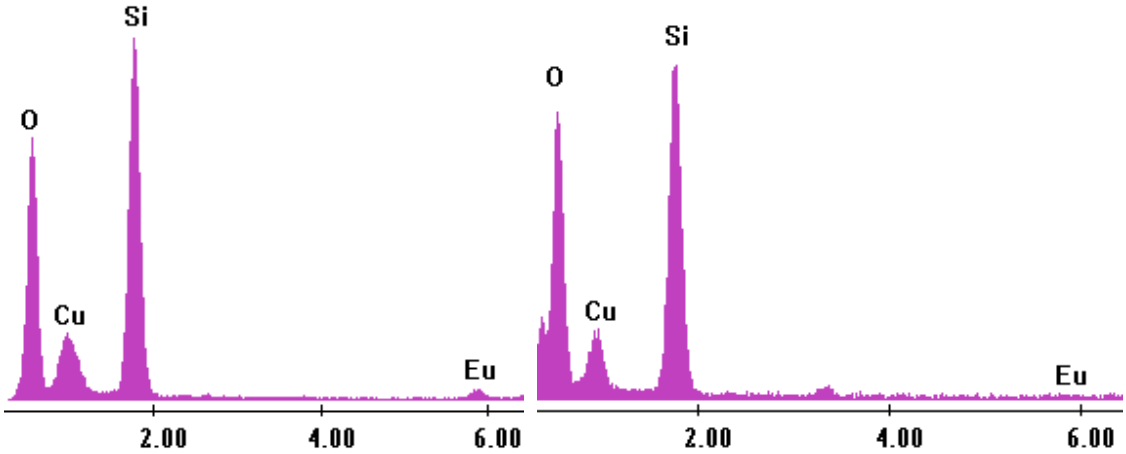


*Figs. 2.14. (a) EDS graph of a cluster of S/EuPic-10 particles and (b) a single particle of the same composites.*

### 2.3.2. TEM of nanocomposites containing silica and mixed complexes.

The mixed complex based nanocomposites were not given much attention but a brief study on two samples show that they are generally spherical. The increased solid loading does not appear to be of negative effect. S/Eu0.3+Tb0.7-8 in particular has a PSR of 29-56 nm, which looks modest when compared to the S/EuPic-8. However, the studies were not detailed and so cannot form the basis for a good comparative analysis, they were only meant to be a quick glance in order to see what the particles look like. EDS analysis on A5 shows the presence of both Tb and Eu.

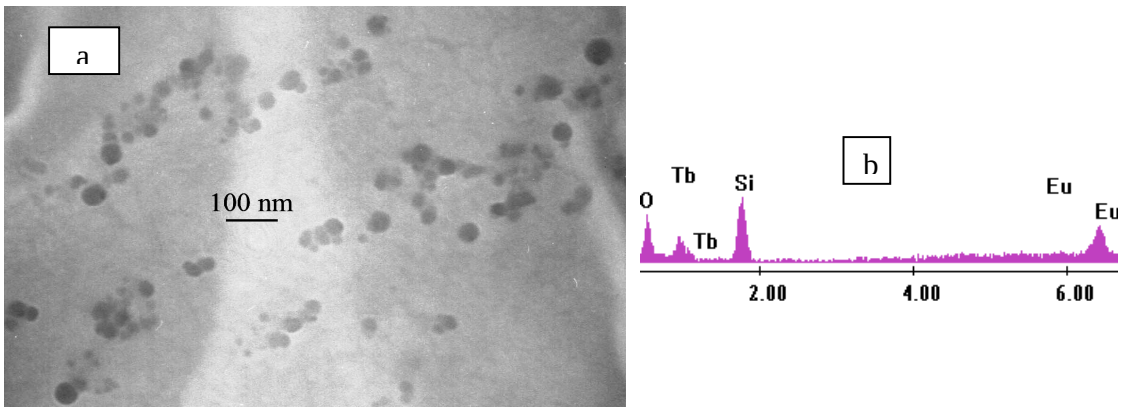


*Figs. 2.15. (a) TEM image of S/Eu0.3+Tb0.7-8; (b) its EDS profile.*

### 2.3.3. TEM of S/0.1Eu-10.

The study on this heterocomplex composite did prove to be the most exciting study on any single sample. The images (figures 2.16 and 2.17) show a multitude of particle with varying sizes and morphology. One interesting observation here which is also seen in TEM images of some of the samples discussed earlier is that particles of similar size and shape at times tend to identify with each other, that is, they have a tendency to form clusters. Whether this is as a

result of the sample preparation steps including the behaviour of the particles in solution, the effect of the grid on the particles or sheer coincidence, cannot be explained at the moment. Since no other heterocomplex based nanocomposite was investigated with TEM, it cannot be said if the development is connected in any way to the nature of the heterocomplexes, but that looks like a remote possibility. The wide size distribution of the sample is in tandem with the observation for higher R values though. The images below are selected for case studies.

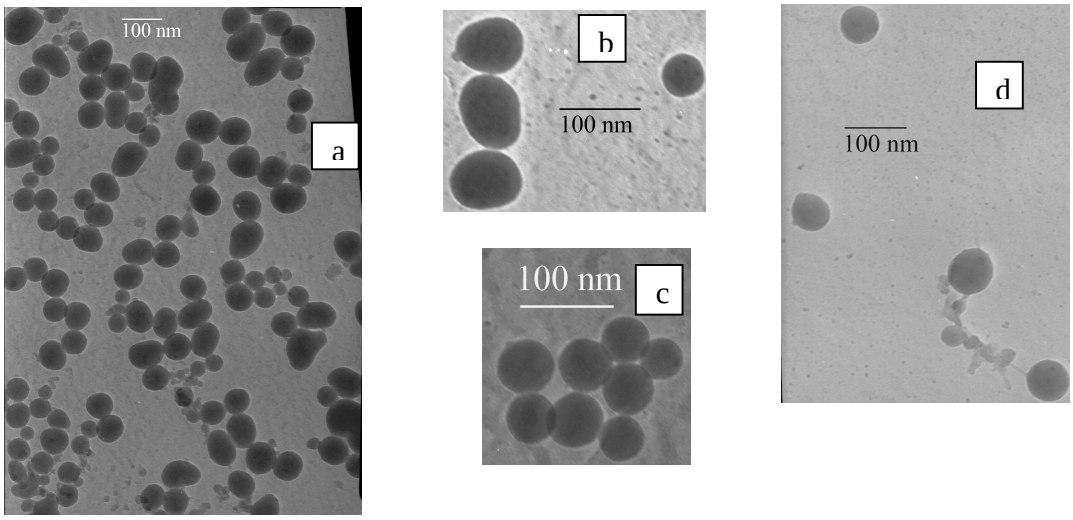


*Figs. 2.16. (a-d)*

Figure 2.16 (a) contains particles that are both spherical and elongated with (longitudinal) diameters ranging from 36 to 90 nm. In figure 2.16 (b), the longitudinal and transverse diameters of the 3 particles arraigned vertically are (from top to bottom) 81 and 67 nm for the first one, 91 and 73 nm for the second, and 87 and 69 nm for the third, respectively. The lone spherical particle at the far right has a diameter of 52 nm. The particles in figure 2.16 (c) are all spherical and can be divide into 3 groups-the smallest- sized group has two particles with APS of 48 nm, the next also has two particles with a diameter of 54 nm while the last has 4

particles with APS of 61 nm. In figure 2.16 (d), all the four particles are spherical and the APS is 67 nm.

All EDS analyses on S/0.1EuPic-10 reveal a significant presence of terbium in addition to silicon but with no sign of europium. This is not totally unexpected as the 0.1EuPic is the heterocomplex with a Tb-Eu mole ratio of 0.9:0.1 in favour of Tb, but it once more underscores the fact that the little and negligible $Tb^{3+}$ luminescence in this study has got nothing to do with the amount of $Tb^{3+}$ ions in the composites.

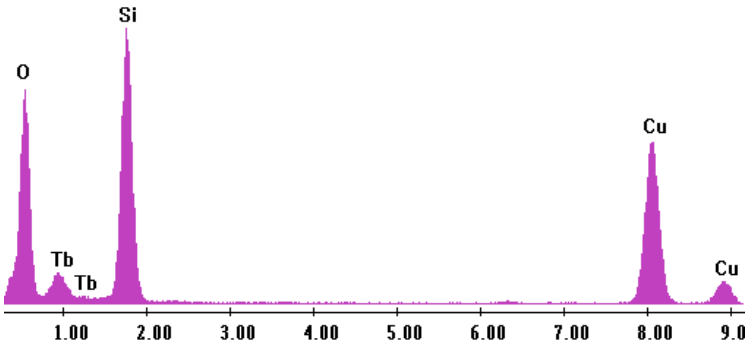


*Fig. 2.17. EDS graph of S/0.1Eu-10.*

### 2.3.4. Particle morphology and intermicellar exchange.

The shapes of quite a number of particles encountered during the TEM studies and more especially in the study on S/0.1Eu-10 give much room to consider how intermicellar exchange might have contributed to having particles that are not spherical and/or very large. In chapter one, intermicellar exchange was established as not only occurring between micelles with only liquid reactants but also between those containing solid particles. Intermicellar exchange begins at the point where two micelles or nanoreactors collide (if we still assume the simple model of binary collision), fuse together, exchange their contents, and then separate again, with the possibility that only one micelle gets all the contents of the two micelles. It can be

inferred with utmost certainty that the possibility of fused micelles being less energetic to exchange their contents and eventually separate is there. This is especially true when the two colliding nanoreactors contain terminal solid particles: The exchange and fission process will be easier between two reactors with liquid content than between two with solid products which might have been fully developed and established in their respective domains. Figure 2.18 below contains a handful of particles that are useful for further elaboration.

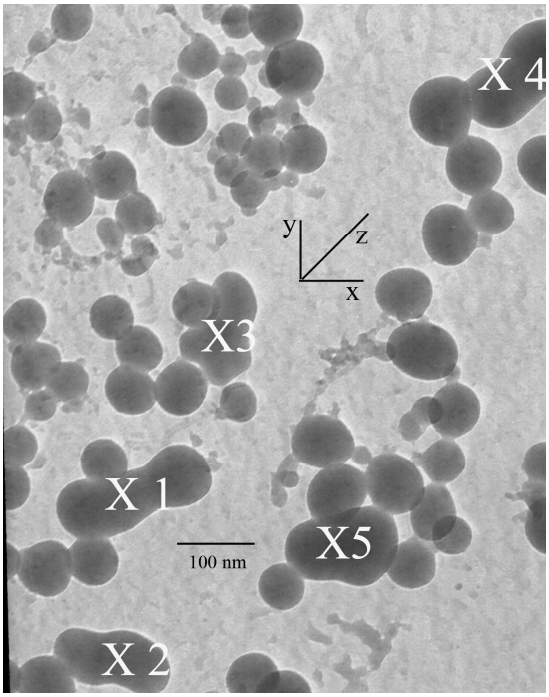


*Fig. 2.18*

Each of the particles marked X1 to X5 are actually made up of more than one particles that have fused together. X2 and X5 can be said to comprise at least two particles fused together along the x-axix. X3 and X4 also seem to consist of two particles fusing together

along the y- and z- axis respectively with X3 appearing like having two other separate particles fused to it along the x-direction. X1 has three particles joined along the z-axis. It looks like fusion steps took place when the individual nanoreactors were almost fully grown and so exchange of contents and fission were impaired or it could be that the nanoreactors were simply unable to separate after fusion. It can also be argued that fission has a competitor in fused micelles preferring to grow together and that the binary collision model is not always followed. X1 and X4, especially the latter, looks very much close to developing into distinct elongated particles. Therefore, the occurrence of larger than “normal” particle sizes and non-spherical shapes in this work can be said to be a result of the fusion of micelles or particles as they collide during synthesis, more so, in a 24 hour, vigorous- stirring experiment. It should be noted that fused particles are not the same as particles that are superimposed on each other or overlapping which can be easily differentiated by the contrast in appearance at the superimposed or overlapping regions.

# Chapter 3. Titania encapsulation of europium complex (T/EuPic).

## *3.1. Synthesis.*

Titania, being a notable bioimplant component, could also be interesting for the encapsulation of luminescent materials for bioapplications. Hence it has been investigated as an alternative encapsulating nanomatrix in this work. The encapsulation of EuPic in titania matrix was carried out by the reverse micelle method as well. Upon addition of titanium (IV) propoxide (TP), the microemulsions instantly turned tickly and homogeneously cloudy, probably indicating that the systems were destabilized at that point.

## *3.2. Photoluminescence.*

Table 3.1 gives a summary of the optical data for $TiO_2$ based nanocomposites.

Table 3.1

| Name | FWHM ($cm^{-1}$) | $^5D_0 \rightarrow {}^7F_0$ ($cm^{-1}$) | $\Delta E\ ^5D_0 \rightarrow {}^7F_1$ ($cm^{-1}$) | RELATIVE INTENSITY 465 nm | 526 nm | 535nm |
|---|---|---|---|---|---|---|
| EuPic | 16.26 | 17248.57 | 208 | 0.15 | | |
| T/EuPic-2 | 33.69 | 17259.65 | 157.13 | 0.88 | 0.15 | 0.23 |
| T/EuPic-4 | 32.52 | 17263.54 | 147.79 | 0.64 | 0.11 | 0.17 |
| T/EuPic-6 | 33.02 | 17261.73 | 158.44 | 0.3 | 0.08 | 0.12 |
| T/EuPic-8 | 32.73 | 17258.54 | 157.58 | 0.27 | 0.1 | 0.12 |
| T/EuPic-10 | 31.95 | 17258.17 | 168.94 | 0.5 | 0.13 | 0.16 |

In comparison with EuPic, the optical features of $Eu^{3+}$ in T/EuPic composites reveal wide changes in titania matrix. The PLE spectra (inset of figure 3.1) of all the composites bear a

very close resemblance to each other, more than the S/EuPic series. Their profiles are all simple and their peak positions only varied from 371 to 374 nm, closer on the average to the 378 nm value of EuPic than the S/EuPic composites. However, the relative intensities of the 465 nm direct europium absorption line are considerably higher than that of the pure complex or any other composites so far discussed. Their values range from 0.27 for R = 8, to 0.88 for R = 2. This does not mean that direct excitation is competing favourably with the ligand-lanthanide synergy as the ligand absorption profile still maintain a broad spectrum as seen in the inset of figure 3.1, and confirmed by the intensity of $Eu^{3+}$ emission upon excitation at 465 nm in figure 3.1 also. Besides the 465 nm line ($^7F_0 \rightarrow {}^5D_2$), there are significant direct excitations at 526 nm ($^7F_0 \rightarrow {}^5D_1$) and 535 nm ($^7F_1 \rightarrow {}^5D_1$). The 535 nm line occasionally appeared in some of the composites discussed before now but the intensities are far less.

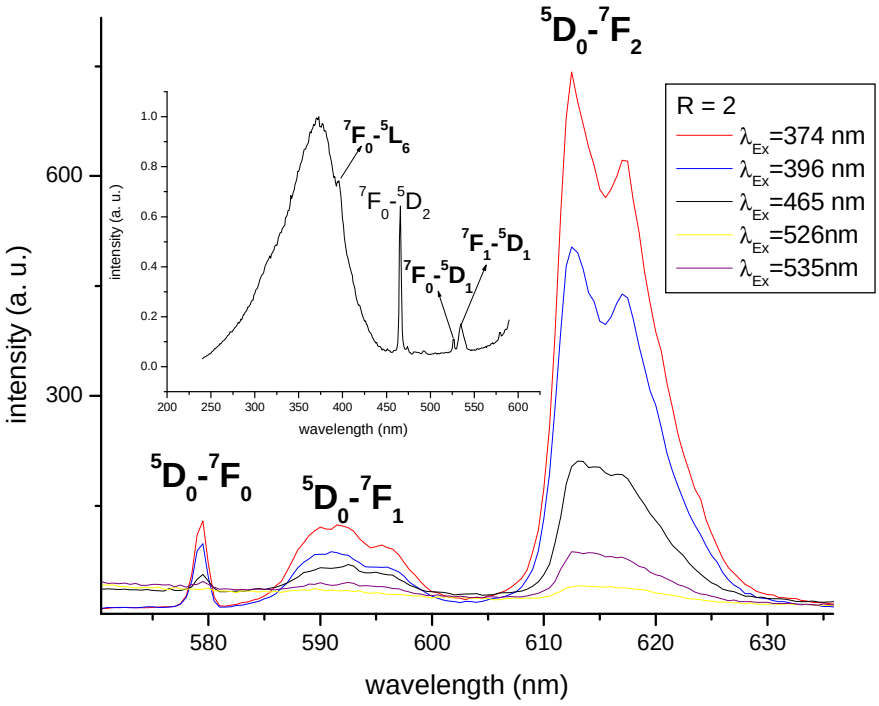


*Fig. 3.1. PL spectra of T/EuPic-2 with excitations at different wavelengths on the PL spectra, including 465, 536 and 535 nm. Inset shows a representative PLE profile.*

The fwhm of each T/EuPic composite is a close approximate of twice the value of that of EuPic. This indicates a wider non-homogeneity of $Eu^{3+}$ local coordination sites in $TiO_2$ than in silica, bringing to fore the question of whether the process is a mere encapsulation as opposed to a sort of chemical reaction between the matrix and the complex leading to extensive modification of the local environment of $Eu^{3+}$. The energy of the $^5D_0 \rightarrow {}^7F_0$ transitions of the composites each increased by more than 9 $cm^{-1}$ above that of EuPic, showing a decrease in covalent character of $Eu^{3+}$ in T/EuPic. The decrease in the $\Delta E {}^5D_0 \rightarrow {}^7F_1$ of the T/EuPic series indicates a lesser crystal field interaction strength than in the pure EuPic. Only two Stark components are observed for the $^5D_0 \rightarrow {}^7F_2$ transition at approximately 613 nm and 617 nm, with the former as the most intense emission line. In general, there are fewer Stark components detected when compared to S/EuPic series and EuPic.

The experimental life time of the excited $^5D_0$ energy level of a representative sample of the series (T/EuPic-10) is 0.298 ± 0.004 ms. This is a decrease from the 0.431± 0.002 and 0.45 ± 0.003 ms values for EuPic and S/EuPic respectively. The efficiency of the $Eu^{3+}$ $^5D_0$ excited state in T/EuPic is 13.1% as against 24.8% and 10.3% for S/EuPic and EuPic respectively.

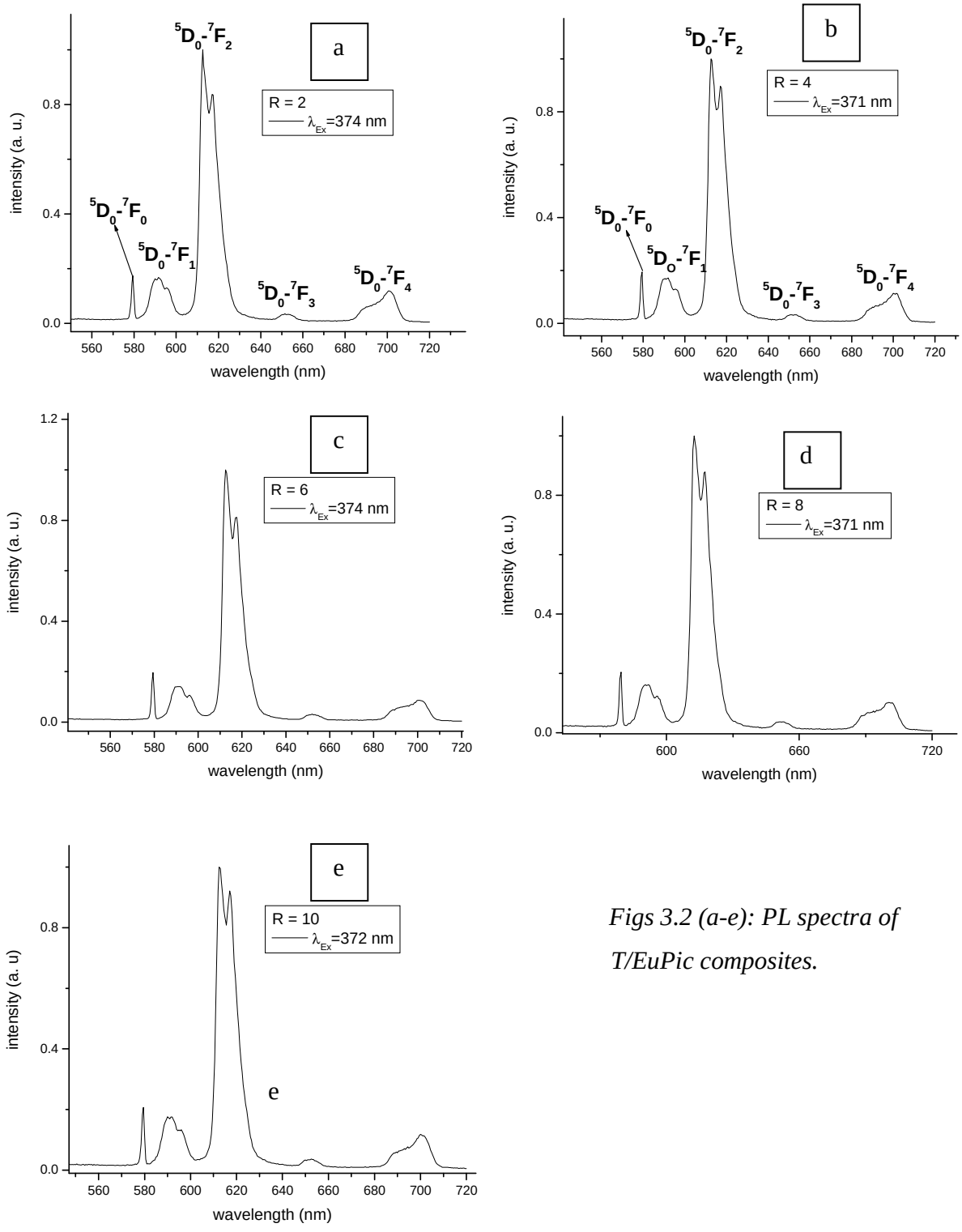


*Figs 3.2 (a-e): PL spectra of T/EuPic composites.*

### *3.3. TEM of T/EuPic series.*

The TEM images of the T/EuPic composites (figure 3.3 a) are similar and reveal what look like a cluster of small particles at low magnification but which appear like a mass of organic layer with no definite particle shape or size at higher magnification. This confirms the suspicion that the system was completely destabilized upon introduction of TP, making it difficult to obtain well defined particles. Due to the high viscosity of TP, it was very difficult to measure an exact amount of it and so the amount used for each experiment was less than 100 µl. EDS analyses reveal a high presence of sodium and sulphur, elements that are not detected in the silica based composites. The Na and S can be said to be coming from the surfactant, AOT, at least partially. This points to a high probability that the product of the synthetic effort to produce T/EuPic is a network of titania, EuPic and AOT with both chemical and physical bonds (samples of T/EuPic-4 and T/EuPic-8 were calcined at 500 °C for 2 hours and sent to the Central Analysis Laboratory at the University of Averio for powder x-ray diffraction analysis. The result turned out to be quite surprising: there was no crystalline $TiO_2$ phase but rather crystalline $Na_2SO_4$).

The use of aqueous sodium chloride to control the synthesis was obviously not very successful (the reaction flask also turned homogeneously cloudy upon addition of TP), the TEM image of the product still shows a mass of seemingly interlinked particles. However, the latter looks a like a better organized disorder than the composites without NaCl (fig. 3.3 b).

a b

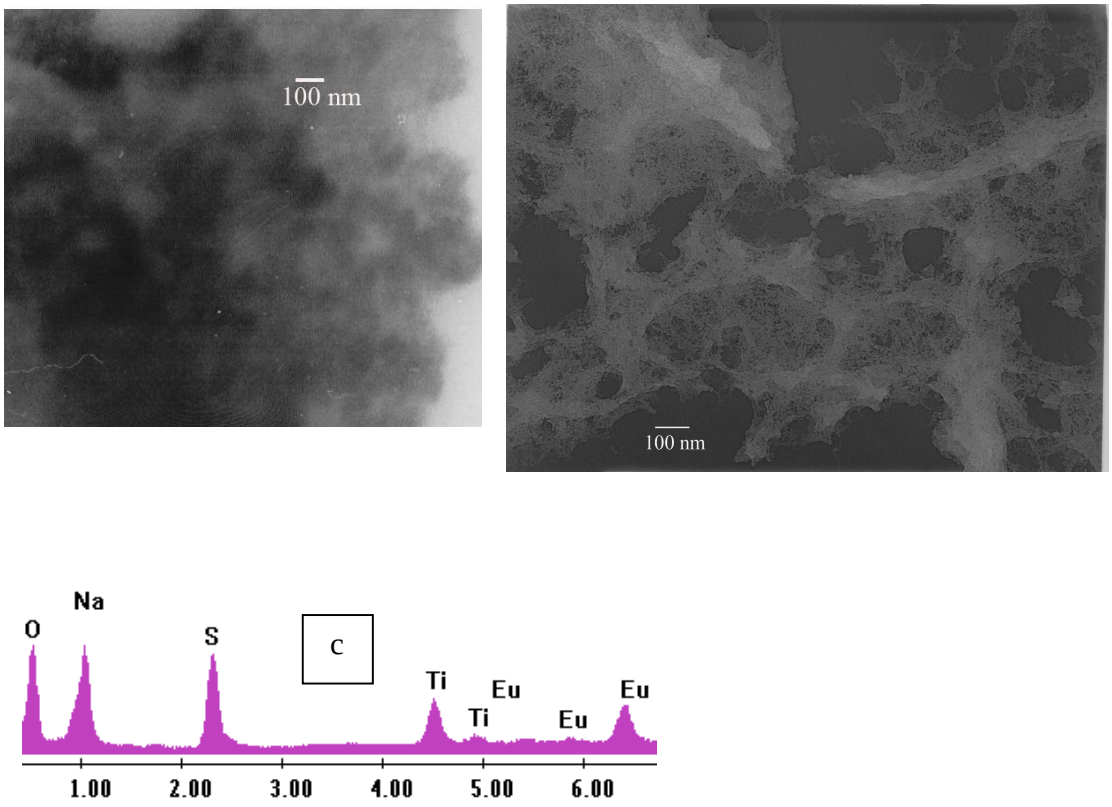


*Figs. 3.3. (a) TEM image of T/EuPic-6, the other members of the series are similar; (b) TEM image of T/EuPic-4 (to which NaCl was added); (c) EDS graph of T/EuPic*

# Chapter 4. Conclusions and future perspectives.

All photoluminescent results of the various categories of nanocomposites confirm the ability of $Eu^{3+}$ to continue to be luminescent in the encapsulating matrixes. However, there are strong indications that the local environments of the ions are modified by the process of incorporating and keeping them inside the enclave of the matrixes. Those changes are quite dynamic and can be exploited for technological adaptation. For example, different lasers can be used as excitation source for the same Eu complex incorporated in the same matrix.

In general, the photoluminescent features of the silica based composites are not affected in any way that will make them unsuitable for the envisaged bioapplication, their actual performance when the particles are in a biological environment will prove the extent of success of this research work. For the T/EuPic, the modifications look very big and this can be correlated to the observation in the synthetic stage of the reaction flask immediately turning homogeneously cloudy on addition of the titania precursor, a possible indication of the destabilization of the entire system and hence the greater tendency of obtaining a highly disordered matrix or $Eu^{3+}$ local environment. The adverse effect on the photoluminescence of $Eu^{3+}$ in titania matrix can be said to be more or less an effect of the matrix when the fact that the T/EuPic composites, unlike the S/EuPic composites, were not subjected to a 24 hour residence in a basic (ammonia) environment.

The wide changes observed in the optical feature of $Eu^{3+}$ ions in titania notwithstanding, a $^5D_0$ excited state lifetime value of 0.298 ± 0.004 ms obtained for T/EuPic is still more than good enough for time resolved fluorescence. Besides, there is a slight increase in the quantum efficiency of the $Eu^{3+}$ $^5D_0$ excited state in titania relative to pure EuPic.

It will be good to adjust the synthetic strategy in future work to see if picolinates complexes of lanthanides will remain usefully luminescent after the synthesis since both the terbium and europium complexes are highly luminescent. An example of the adjustment of the synthetic step could be the use of milder basic catalyst like tertiary amine or the use of acidic catalyst or any other agent that could promote the hydrolysis of TEOS without adversely affecting the luminescence of the complex.

There are significant hopes raised on the possibility of an energy transfer from$Tb^{3+}$ to

$Eu^{3+}$ judging from the relative intensities of the 465 nm direct europium excitation line in the heterocomplexes and the existence of an absorption band at 486 nm in the PLE of the heterocomplexes and S/TbPic series. In addition, the possibility of the ligand absorption, and not only the $Eu^{3+}$ local environment, being subject to changes by the synthetic steps, has also been raised.

TEM studies confirm that increasing nanoparticle size is obtained with increasing R value in a reverse micelle system. R = 4 in this thesis research has proved to be the most suitable for producing monodispersed spherical particles. The presence of very large and/or non-spherical particles can be justified based on the concept of intermicellar exchange or fusion. EDS analyses suggest that the almost lack of luminescence from $Tb^{3+}$ has nothing to do with the absence of the ions in the composites. The morphology of T/EuPic composites and EDS analyses on them lend support to argument that the destabilization of the reaction system upon addition of TP led to the formation of an organic rich and highly disordered material which affected the luminescence of $Eu^{3+}$ ions. Good control over the synthesis of T/EuPic composites is not likely to be achieved using this reverse micelle method, the mixing of two microemulsion approach especially with the titanium alkoxide dissolved in an alcohol (e.g. ethanol) can be handy in controlling the rate of hydrolysis of TP.

The preparation of particles with an average diameter of 31nm and below and which show fairly good monodispersity in this research effort demonstrates the suitability of reverse micelle for producing monodispersed particles which are less than 100 nm. This is often a limitation inherent in using sol-gel method to produce ceramic nanoparticles. An earlier work to prepare silica nanoparticles encapsulating EuPic at the University of Aveiro by sol-gel method led to particles with an average diameter above 100nm and which were much agglomerated [4]. However, it will still be nice in future work to study the optimal reaction parameters-solid loading, amount of catalyst, stirring rate- that will give the best of results for the classes of nanoparticles made here. A future work on the kinetics of reverse micelle, especially as it concerns intermicellar exchange or fusion, will also be useful and could perhaps provide a clue to making nanorods of the composites. Even though nanoparticles in the smaller size range (< 50 nm) are often reported as being more suited for *in vivo* application, the larger ones (even up to micron size) have been reported as being more

significant in certain applications [108]. Therefore, the production of large particles in this work can also be an advantage.

Although the emphasis of this work is on developing nanosized materials for bioapplication, the successful incorporation of lanthanide complexes in nanosized silica can also be interesting for applications in optical fibres, light emitting diodes, luminescent displays, and lamps [113]. The small size of the particles make them particularly promising for high resolution displays like plasma display panel and field emission display which may work on low energy excitation source. Phosphors for such display application are required to consist of small particles and using conventional physical processes (ball milling for instance) to reduce the particle sizes of phosphors has been reported to lead to poor phosphor luminescence due to the formation of surface defects [12, 15, 112]. Also, small particles are said to improve aging by forming densely packed layers [15]. In fact, the preparation of (doped) oxides nanoparticles of lanthanides has been receiving some good attention in recent times [7, 12, 15, 114]. In addition, the nanoparticles made here can be relied on to be stable in high vacuum and oxygen environment since they are oxides. Even with this optimism, it will be nice to investigate the luminescence behaviour of the nanocomposites in low voltage, higher than room temperature, and oxygen rich environment in future work in order to appreciate the luminescent potentials of the nanocomposites further.

# Chapter 5. Experimental

## *5.1. Synthesis.*

All chemicals were supplied by Aldrich and used as received.

Water-in-oil microemulsions were prepared by measuring 10ml heptane into a 25ml round bottom flask, followed by addition (stirring) of 0.6g AOT. Still under vigorous stirring, varying volumes of distilled water were added to the flask, the volume added in each experiment depending on the R value (see table for the volumes of water for different R values ).

Table 5.1

| R | Amount of Water (µl) |
|---|---|
| 2 | 50 |
| 4 | 100 |
| 6 | 150 |
| 8 | 200 |
| 10 | 245 |

Next, 20 to 100 µl of a dimethyl sulfoxide (DMSO) or aqueous solution of the lanthanide complexes were added. The total amount of lanthanide complex used was 5 mg for all nanocomposites series except the mixed complexes based silica nanocomposite which contained a total of 10 mg of a mixture of EuPic and TbPic; in addition, S/EuPic-2, S/EuPic-3 and S/EuPic-4 contained 2, 3, and 4 mg of EuPic respectively. The addition of lanthanide

complexes was followed by the addition of 100 µl of TEOS in the case of silica or TP in the case of titania based composites. In the case of silica based nanocomposites, 100 µl of 25% aqueous ammonia was added to catalyse the hydrolysis of TEOS. Dilute hydrochloric acid was employed as a catalyst/aid for the synthesis of T/EuPic but was discontinued after it became obvious that it severely diminished the luminescence of the complex.

The reaction flask for the synthesis of the silica-lanthanide nanocomposites (S-L) were stirred for 24 hours after the last reagent was added while that for the titania-lanthanide nanocomposite (T-L) was stirred for two hours. In each case, the stirring was maintained at 600 1/min from the addition of AOT right to the end, and the steps from the addition of distilled water to the addition of aqueous ammonia (in the case of S-L) or to the addition of TP (in the case of T-L) had 5-7 minutes interval between them.

At the end of the stirring period, the S-L nanoparticles were precipitated out by the addition of acetone while the T-L nanoparticles needed no such step. The nanoparticles were then separated by centrifuging and washed twice with heptane and ethanol each. Further washing with 1-propanol, 1-butanol, and ethanol or 1-propanol, 1-butanol, ethanol, and distilled water was done when considered necessary for transmission electron microscopy.

The added DMSO solution containing the lanthanide complex was either that of:

a. 3-hydroxypicolinate or picolinate of europium or terbium
b. A mixture of the 3-hydroxypicolinate of Eu and Tb in varying proportion
c. Hetero-complexes of 3-hydroxypicolinate or picolinate of Eu and Tb in varying theoretical ratios (that is the two lanthanides are contained in the same molecular complex)

Generally, the luminescence of the lanthanide-picolinate complexes were drastically reduced after the synthesis and so further work on them was discontinued.

The synthesis of the lanthanide complexes (outside the scope of this work) was carried out by Dr. Paula Soares Santos as reported elsewhere [4]. Typically, $Ln(OH)_3$ (Ln = Eu, Tb ) was prepared by adding aqueous solutions containing KOH (8ml, 1.5 mmol) to an equal volume of aqueous solutions of the lanthanide chloride salt (1.5 mmol). The solid product was stirred over 90 min, filtered, and washed thoroughly with distilled water. The 3-hydroxypicolinate lanthanide complexes were prepared by adding 1 mmol of $Ln(OH)_3$ to an aqueous solution

containing 3-hydroxypicolinic acid (25 ml, 4 mmol). The mixture was stirred for 1 h, and then heated for 30 min at 80 °C, followed by further stirring over 8 h at room temperature. The solid obtained was filtered, washed thoroughly with distilled water, and dried over silica gel. The heterocomplexes were prepared by utilizing the appropriate mixture of the lanthanide hydroxides in accordance with the intended ratio in each heterocomplex.

## *5.2. Photoluminescence.*

The Photoluminescence excitation (PLE) spectra were obtained at 300 K on a Jobin Yvon-Spex spectrometer (HR 460) coupled to a R928 Hamamatsu photomultiplier, under continuous excitation of a Xe arc lamp (150 mW). The excitation monochromator is a Jobin Yvon (TRIAX 180). The spectra were corrected for the response of the detector. Emissions were monitored at 544 and 612 nm for $Tb^{3+}$ and $Eu^{3+}$ respectively, except otherwise indicated.

The photoluminescence (PL) and lifetime measurements were recorded at 300 K on a modular double grating excitation spectrofluorimeter with a TRIAX 320 emission monochromator (Fluorolog-3, Jobin Yvon-Spex) coupled to a R928 Hamamatsu photomultiplier, using the front face acquisition mode. All the photoluminescence spectra were corrected for optical and detection spectral responses. Life times were determined around the most intense emission line of each $Eu^{3+}$ with the corresponding excitation wavelength, and the decay profiles were well reproduced by single exponentials. Quantum efficiency, *q*, of the excited $^5D_0$ state of $Eu^{3+}$ was calculated based on the following [4, 111]:

$$q = k_r/(k_r + k_{nr}), \qquad 5.1$$

where $k_r$ and $k_{nr}$ are radiative and non-radiative transition probabilities respectively and the value of their sum is the inverse of the life time of the excited state. $k_r$ is given by:

$$k_r = A_{0\rightarrow1}\,(\hbar\omega_{0\rightarrow1}/S_{0\rightarrow1})\sum_{J=0}^{4}(S_{0\text{-}J}/\hbar\omega_{0\text{-}J}), \qquad 5.2$$

Where $A_{0\rightarrow1}$ is the Einstein's coefficient of spontaneous emission between the $^5D_0$ and the $^7F_1$ energy levels and is value is approximately 50 $s^{-1}$. The notations $\hbar\omega$ and $S$ stand for transition energy and the integrated intensity of an emission curve respectively. Some basic assumptions made in this calculation are that only radiative and non-radiative processes are involved in the depopulation of the $^5D_0$ state and that the contribution of the $^5D_0 \rightarrow {}^7F_{5,\,6}$ transitions to the depopulation of the $^5D_0$ state are negligible.

## *5.3. Transmission electron microscopy*

Transmission electron microscopy study of the morphology of the nanoparticles was carried out with a Philips electronic EM400T microscope at an accelerating voltage of 100-120 eV. The microscope was coupled to EDAX Genesis software with an ultra thin window (UTW) detector for energy dispersive x-ray spectroscopy (EDS). Samples were prepared by dipping carbon coated copper grids in dilute heptane solutions of the composites. Average particle sizes were determined by statistical calculation based on TEM images alone.

## References


1. Blasse, G.; Grabmaier, B. C.; *Luminescent Materials*, Springer,Verlag Berlin Heidelberg, (1994), Ch. 1 to 4.
2. Bunzli, J.-C. G.; Piguet, C. *Chem. Soc. Rev.*, (2005), 34, 1048
3. Soares-Santos, P. C. R.; Nogueira, H. I. S.; Paz, F. A. A.; Ferreira, R. A.S.; Carlos, L. D.; Klinowski, J.; Trindade, T. *Eur. J. Inorg. Chem.*, (2003), 3609.
4. Soares-Santos, P. C. R.; Nogueira, H. I. S.; Felix, V.; Ferreira, R. A. S.; Carlos, L. D.; Drew, M. G. B.; Trindade, T. *Chem. Mater.*, (2003), 15, 100.
5. Meyssamy, H.; Riwotzki, K.; Kornowski, A.; Naused, S.; Haase, M. *Adv. Mater.*, (1999), 11, 840.
6. Platas-Iglesias, C.; Piguet, C.; Andre, N.; Bunzli, J.-C. G. *J. Chem. Soc., Dalton Trans.*, (2001), 3084.
7. Dosev, D.; Nichkova, M.; Liu, M.; Gou, B.; Liu, G.-Y.; Hammock, B. D.; Kennedy, I. M. *J. Biomed. Optics*, (2005), 10, 1.
8. Case, P. J.; Harper, A. W. *Mat. Res. Soc. Symp. Proc.*, (2003), 771, L4.10.1-L4.10.2.
9. Soares-Santos, P. C. R.; Nogueira, H. I. S.; Felix, V.; Ferreira, R. A. S.; Carlos, L. D.; Drew, M. G. B.; Trindade, T. *Inorg. Chem. Commun.*, (2003), 6, 1234.
10. Creating Solutions for the future of Science-Using the Synergy HT to measure Time-Resolved Fluorescent Compounds. Bio-Tek Instruments, www.biotek.com
11. Hong. G. Y.; Yoo, K.; Moon, S. J.; Yoo, J. S. *J. Electrochem. Soc.*, (2003), 150, 67.
12. Hutchison, J. L.; Dobson, P. J.; Keron, H. A.; Wakefield, G. *J. Phys. Chem. Solids*, (1999), 60, 503
13. Soares-Santos, P. C. R.; Nogueira, H. I. S.; Felix, V.; Ferreira, R. A. S.; Carlos, L. D.; Rocha, J.; Drew, M. G. B.; Trindade, T. *Polyhedron*, (2003), 22, 3529.
14. Korenowski, G. M.; Sheng, K. C. J. *Phys. Chem.*, (1988), 92, 50.
15. Park, H. D.; Kim, E. J.; Roh, H. S.; Kang, Y. C. *J. Electrochem. Soc.*, (2003), 150, 93.
16. Faucher, M.; Dexpert-Ghys, *J. Phys. Rev. B*, (1979), 20, 10.
17. Vergeer, P.; Vlugt, T. J. H.; Kox, M. H. F.; den Hertog, M. I.; van der Eerden, J. P. J.

M.; Meijerink, *A. Phys. Rev. B,* (2005), 71, 141191.

18. Davolos, M. R.; Stucchi, E. B.; da Vila, L. D. *J. Mater. Chem.,* (1997), 7, 2113.
19. Driessen, A.; Worhoff, K.; Diemeer, M. B. J.; Borreman, A.; Klunder, D. J. W.; Dekker, R.; van Veggel, F. C. J. M.; Stouwdam, J. W. *Appl. Phy. Lett.,* (2004), 85, 6104.
20. Nann, T.; Darbandi, M. *Chem. Commun.,* (2006), 776.
21. Gudel, H.U.; Kramer, K. W.; Trupke, T.; Richards, B. S.; Shalav, A.; *Appl. Phys. Lett.* (2005), 86, 135051.
22. Gudel, H.U.; Kramer, K. W.; Grimm, J.; Suyver, J. F. *J. Lumin.,* (2005), 114, 53.
23. Haase, M.; Gudel, H. U.; Kompe, K.; Heer, S. *Adv. Mater.,* (2004), 16, 23.
24. Soukka, T.; Kuningas, K.; Rantanen, T.; Haaslahti, V.; Lovgren, T. *J. Fluoresc.,* . (2005), 15, 513.
25. Abdel-Mottaleb, M. S.A.; Bakier, E. *Int. J. Photoenergy,* (2005), 7, 51.
26. Parker, D.; Yu, J.; Pandya, S. *Dalton. Trans.,* (2006), 2757.
27. Murner, H.-R.; Scopelliti, R.; Bunzli, J.-C. G. *Acta. Cryst.,* (2002), 58, 434.
28. Binnemans, K.; Gorller-Walrand, C.; Lenaerts, P. *J. Lumin.,* (2006), 117, 163.
29. Liu, Y.; Ye, C.; Qian, G.; Qiu, J.; Wang, M.; *J. Lumin.,* (2006), 118, 158.
30. Guillet, E.; Imbert, D.; Scopelliti, R.; Bunzli, J.G. , *Chem. Matter.,* (2004), 16, 4063.
31. Ward, M. D.; Faulkner, S.; Adams, H.; Jeffery, J. C.; Motson, G. R.; Aarons, R. J.; Davies, G. M. *Dalton. Trans.,* (2004), 1136.
32. Ward, M. D.; Faulkner, S.; Pope, S. J. A.; Adams, H.; Davies, G. M. *Photochem. Photobiol. Sci.,* (2005), 4, 829
33. Petoud, S.; Geib, S. J.; Badger, P. D.; Zhang, *J. Angew. Chem. Int. Ed.,* (2005), 2508.
34. Jaakkola, L.; Peuralahti, J.; Hakala, H.; Mukkala, V.-M.; Hurskainen, P.; Hovinen, J. *J. Peptide Sci.,* (2006), 12, 199.
35. Matsumoto, K.; Yuan, J.; Wang, Z. *Luminescence,* (2005), 20, 347.
36. McGehee, M. D.; Bergstedt, T.; Zhang, C.; Saab, A. P.; O'Regan, M. B.; Bazan, G. C.; Srdanov, V. I.; Heeger, A. *J. Adv. Mater.,* (1999), 11, 1349.
37. Yang, S.; Williams, S. A.; Vallarino, L. M.; Bromm Jr, A. J.; Becker, M. C.; Leif,

R. C. *Soc. Photo-Opt. Instrum. Eng. BIOS Proc.*, (2006), 4260, 1.

38. Suarez, S.; Mamula, O.; Imbert, D.; Piguet, C.; Bunzli, J.-C. G. *Chem. Commun.*, (2003), 1226.
39. Faul, C. F. J.; Antonietti, M.; Spitz, C.; Zhang, T. *Chem. Eur. J.*, (2005), 11, 1001.
40. Phillips, D. L.; Wong, W.-T.; Kwok, W.-M.; Law, G.-L.; Wong, K.-L. *Angew. Chem. Int. Ed.*, (2005), 44, 3436.
41. Kentgens, A. P. M.; van Blaaderen, A. *J. Non-Cryst. Solids*, (1992), 149, 161.
42. Brittain, W. J.; Ranjan, R.; Radhakrishnan, B.; *Soft Matter*, (2006), 2, 386.
43. Kisch, H.; Janczarek, M.; Sakthivel, S. *J. Phys. Chem. B*, (2004), 108, 19384.
44. Colbeau-Justin, C.; Mazerolles, L.; Kunst, M.; Churagulov, B. R.; Kolen'ko, Y. V. *Appl. Catal. B*: *Environ.*, (2004), 54, 51.
45. Mallouk, T. E.; Fendler, J. H.; Cassagneau, T. *Langmuir*, (2000), 16, 241.
46. Hirao, K.; Shi, W.; Dai, K.; Zhao, D.; Peng, T. *J. Phys. Chem. B*, (2005), 109, 4947.
47. Maret, G.; Widoniak, J.; Eiden-Assmann, S. *Chem. Mater.*, (2003) (American chemical society, Published on Web 00/00/0000 PAGE EST: 5.2)
48. Sayilkan, H.; Sayilkan, F.; Sener, S.; Erdemoglu, S.; Akarsu, M.; *Turk. J. Chem*, (2004), 28, 27.
49. Spencer, N. D.; Textor, M.; Schlottig, F.; Mark, G.; Schreckenbach, J. P. *J. Mater. Sci: Materials in Medicine*, (1999), 10, 453.
50. Luo, D.; Saltzman, W. M. *Gene Therapy*, (2006), 13, 585. http://www.nature.com/gt/journal/v13/n7/full/3302662a.html
51. Qutubuddin, S.; Fu, X. *Colloids and Surfaces. A: Physicochem. Eng. Aspects*, (2001), 179, 65.
52. Dong, S.; Li, Z.; Cheng, G.; Wu, A.; Wang, B.; Jia, *J. Anal. Chem.*, (2002), 74, 2218.
53. Barbe, C.; Gorissen, E.; Calleja, S.; McNiven, S.; Lin, H.-Q.; Jacques, D.; Kong, L.; Finnie, K. *Chemistry in Australia*, (2005), 13.
54. Bright, F. V.; Colon, L. A.; Gardella Jr, J. A.; Zhuang, H.; Hook, D. J.; Dunbar, R. A.; Jordan, J. D. *Chem. Mater.*, (1998), 10, 1041.
55. Bravo-Zhivotovskii, D.; Melamed, S.; Apeloig, Y.; Schmidt, A.; Melchior, S.; Shter,

G. E.; Grader, G. S. *Chem. Mater.*, (2001), 13, 247.

56. Rahman, I. A.; Hamid, M. A. *Malays. J. Chem.*, (2003), 5, 86.

57. Nann, T.; Thomann, R.; Darbandi, M. Chem. Mater., (2005), (American chemical society, Published on Web 00/00/0000 PAGE EST: 5.7)
58. Hozumi, A.; Okudera, H. *Thin Solid Films*, (2003), 434, 62.
59. Maitra, A.; Ayyub, P.; Chhabra, V.; Lal, M. *J. Mater. Res.*, (1998), 13, 1249.
60. Meier, W. Curr. Opinion. Coll. *Interf. Sci.*, (1999), 4, 6.
61. Nagy, J. B.; Masereel, B.; Jeunieau, L.; Cuisenaire, J.; Debuigne, F.; *J. Coll. Interf. Sci.*, (2001), 243, 90.
62. Bagwe, R. P.; Wang, L.; Drake, T.; Zhao, X. J.; He, X.; Wang, K.; Tan, W. *Med. Res. Rev.*, (2004), 24, 621.
63. Khilar, K. C.; Mehra, A.; Hota, G.; Kumar, A. R. *AIChE Journal*, (2004), 50, 1556.
64. Sundmacher, K.; Adityawarman, D.; Voigt, A. *Nanotechnology*, (2005), 16, 429.
65. Tan, W.; Zhang, P.; Santra, S.; Qhobosheane, M. *Analyst*, (2001), 126, 1274.
66. Santucci, A.; Onori, G.; Mannaioli, S.; Freda, M.; Fioretto, D. *J. Phys. Chem. B*, (1999), 103, 2631.
67. Bark, K.-M.; Yang, K.; Lee, J.-K.; Kim, T. H.; Lee, H.-C.; Park, H.-R. *Photochem. Photobiol.*, (2000), 71, 281.
68. Rinaldi, C.; Briano, J. G.; Resto, O.; Herrera, A. P. *Nanotechnology*, (2005), 16, 5618.

69a. Leng, F. J.; Heenan, R. K.; Towey, T. F.; Robinson, B. H.; Fragneto, G.; Eastoe, J. *J. Chem. Soc. Faraday Trans.*, (1992), 88, 461.

69b. http://66.249.93.104/search?q=cache:http://www.chm.colostate. edu/bl/res03.htm&hl=en&lr=&strip=1), accessed on 15/07/2007

70. Gan, L. M.; Ng, S. C.; Wang, J.; Ng, W. B. *J. Am. Ceram. Soc.*, (1999), 82, 529.
71. Zhang, L.; Zhang, Y.; Zhang, J.; Li, G.; Zhang, B. *Nanotechnology*, (2003), 14, 443.

72. Khilar, K. C.; Bagwe, R. P. *Langmuir*, (2000), 16, 905.
73. Nann, T.; Fang, J.; Lu, W.; Darbandi, M. *Langmuir*, (2006), (American chemical society, Published on Web 03/31/2006 PAGE EST: 4.6)
74. Mehra, A.; Shukla, D. *Nanotechnology*, (2006), 17, 261.
75. Kopelman, R.; Anker, J. N.; Roberts, T. G. *J. Magnet. Magnet. Mater.*, (2005), 293, 715.
76. Makowska, B.; Elbanowski, M. *J. Photochem. Photobiol. A*, (1996), 99, 85.
77. Norgaard, L.; Ladefoged, A. M.; Christensen, J. *J. Inst. Brew.*, (2005), 111, 3.
78. Wang, M.; Fan, X.; Zhang, Y.; Tan, W. B.; Wang, F. *Nanotechnology*, (2006), 17, 1.
79. Trindade, T.; Pickett, N. L.; O'Brien, P. *Chem. Mater.*, (2001) 13, 3843.
80. Sapra, S.; Sarma, D. D.; Sanvito, S.; Hill, N. A. *Nano Lett.*, (2002), 2 , 605.
81. Gao, X.; True, L.; Nie, S.; Dave, S.; Smith, A. M. *Expert Rev. Mol. Diagn.*, (2006), 6, 231.
82. Mericle, R. A.; Moudgil, B. M.; Tan, W.; Cao, Z.; Dutta, D.; Bertolino, C.; Liesenfeld, B.; Santra, S. *J. Lumin.*, (2006), 117, 75.
83. Hardman, R. *Environ. Health Perspectives*, (2006), 114, 165.
84. Roy, A.; Singha, A. *J. Mater. Res.*, (2006), 21, 1385.
85. Wang, P. N.; Xu, L.; Yang, W. L.; Wang, C. C.; Guo, J.; Chen, J.-Y, Ma, J. *Nanotechnology*, (2006), 17, 2083.
86. Moss, S. C.; LaLumondiere, S. D.; Jennings, T. L.; Speckman, D. M. *Mat. Res. Soc. Symp. Proc.*, (2002), 704, W9.19.1-W9.19.2
87. Selvin, P. R.; Ge, P. *Bioconjugate Chem.*, (2003), 14, 870.
88. Faulkner, S.; Snaith, J. S.; Kauppinen, R. A.; Spencer, N.; Allan, S.; Narvainen, J.; Vidyasagar, R.; Feng, J.; Meloni, M. M.; Notta, J. K.; Aarons, R. J. *Chem. Commun.*, (2006), 909.
89. Slater, R.; Parker, D.; Cann, M. J.; Bretonniere, Y. *Chem. Commun.*, (2002), 1930.
90. Diamandis, E. P.; Pollak, A.; Dickson, E. F. G. *J. Photochem. Photobiol.*, (1995), 27, 3.

91. Lovgren, T.; Soukka, T.; Harma, H. *Clin. Chem.,* (2001), 47, 561.
92. Takalo, H.; Lovgren, J.; Eriksson, S.; von Lode, P.; Pettersson, K. *Point of Care*, (2003), 2, 225.
93. Lovgren, T.; Torresani, T.; Iitia, A.; Heinonen, P. *Clin. Chem.,* (1997), 43, 1142.
94. Faulkner, S.; Pope, S. J.A.; Burton-Pye, B. P. *Appl. Spectrosc. Rev.* (2005), 40, 1.
95. Kennedy, I. M.; Hammock, B. D.; Gee, S. J.; Stephanian, A.; Koivunen, M. E.; Cummins, C. M. *Biosens. Bioelectro.,* (2006), 21, 1077.
96. Lovgren, T.; Mikola, H.; Hemmila, I.; Blomberg, K.; Pettersson, K.; Xu, Y.-Y. *Clin. Chem.,* (1992), 38, 2038.
97. Christopoulos, T. K.; Ioannou, P. C. *Anal. Chem.,* (1998), 70, 698.
98. Bao, G.; Xu, Y.; Behlke, M. A.; Tsourkas, A. *Anal. Chem.,* (2003), 75, 3697.
99. Wang, L. V.; Stoica, G.; O'Neal, D. P.; Gill, K. L.; Ku, G.; Wang, X.; Xie, X.; Wang, Y. *Nano Lett.,* (2004), 4, 1689.
100. Mathis, G.; Trinquet, E.; Bazin, H. *Rev. Mole. Biotechn.,* (2002), 82, 233.
101. Wang, T.-H.; Shih, I.-M.; Ho, Y.-P.; Yeh, H.-C. *Nucl. Acids Res.,* (2006), 34, 1.
102. Strano, M. S.; Gastala, J. B.; Roy, A. C.; Moll, A. E.; Jeng, E. S. *Nano Lett.,* (2006), 6, 371.
103. Rotello, V. M.; Verma, A.; You, C.-C. *Soft Matter,* (2006), 2, 190.
104. T. Vo-Dinh, F. Yan & M. B. Wabuyele, *J. Raman Spectrosc.,* (2005), 36, 640.
105. A. J. Haes, C. L. Haynes, A. D. McFarland, G. C. Schatz, R. P. V. Duyen & S. Zou, *MRS Bull.,* (2005), 30, 368.
106. Kennedy, I. M.; Hammock, B. D.; Gee, S. J.; Dosev, D.; Nichkova, M. *Anal. Chem.,* (2005), 77, 6864.
107. Roux, C.; Coradin, T.; Livage, J. *J. Phys.: Condens. Matter,* (2001), 13, 673.
108. Drofenik, M.; Kosak, A.; Uskokovic, V. Int. *J. Appl. Ceram. Technol.,* (2006), 2, 135.
109. Wiesner, U.; Webb, W. W.; Baird, B. A.; Srivastava, M.; Larson, D. R.; Ow, H. *Nano Lett.,* (2005), 5, 113.
110. Yuan, J.; Ye, Z.; Wang, G.; Tan, M. *J. Lumin.,* (2006), 117, 20.
111. Fernandes, J. A.; Ferreira, R. A. S.; Pillinger, M.; Carlos, L. D.; Jepsen, J.;

Hazell, A.; Ribeiro-Claro, P.; Goncalves, I. S. *J. Lumin.*, (2005), 113, 50.

112. Carlos, L. D.; Malta, O. L.; Albuquerque, R. Q. Chem. Phys. Lett., (2005), 415, 238.
113. Costa, C. C.; Vasconcelos W. L.; Bray, K. L. *Quimica Nova*, (1998), 21, 374.
114. Wakefield, G.; Keron, H. A.; Dobson, P. J.; Hutchison, J. L. *J. Coll. Interf. Sci.*, (1999), 215, 179.